PONTIFICIA UNIVERSIDAD CATOLICA DE CHILE
ESCUELA DE INGENIERIA

EVALUATION OF THE EFFECT OF FIBER MORPHOLOGY AND THE PRESENCE OF DECORIN IN THE CELLULAR RESPONSE OF MYOBLASTS ON POLYMER FIBER SCAFFOLDS OBTAINED BY ELECTROSPINNING

PHAMMELA N. ABARZUA

Thesis submitted to the Office of Research and Graduate Studies in partial fulfillment of the requirements for the Degree of Master of Science in Engineering

Advisor:
LORETO VALENZUELA
HUGO OLGUIN

Santiago de Chile, (September, 2016)

PONTIFICIA UNIVERSIDAD CATOLICA DE CHILE
ESCUELA DE INGENIERIA

EVALUATION OF THE EFFECT OF FIBER MORPHOLOGY AND THE PRESENCE OF DECORIN IN THE CELLULAR RESPONSE OF MYOBLASTS ON POLYMER FIBER SCAFFOLDS OBTAINED BY ELECTROSPINNING

PHAMMELA NOEMI ABARZUA ILLANES

Members of the Committee:

LORETO VALENZUELA

HUGO OLGUIN

TOMAS EGAÑA

JUAN PABLO ACEVEDO

MIGUEL NUSSBAUM

Thesis submitted to the Office of Research and Graduate Studies in partial fulfillment of the requirements for the Degree of Master of Science in Engineering

Santiago de Chile, September, 2016

To my parents, sisters, boyfriend and friends who were always there to support me; and to my cat who always stayed up with me on my all-nighters.

ACKNOWLEDGMENTS

I would like to thank my professor Loreto Valenzuela for teaching, guiding and supporting me every step of the way. To Hugo Olguín who taught me so much about the biological aspects of my project and who let me use his facilities to culture my cells. A special thank you for Hugo's laboratory students who taught me everything I now know in the lab. Thanks for your time and patience and the good times. Thank you to Stefan Nieldbalski who lent so much of his time to measure my samples in the DSC. To Leonard Molero who helped me measure my fibers in the AFM for many hours, even spending his weekends and off hours; I don't think any number of brownies can say how grateful I am. To Cristina Padilla who helped me with all the lab procedures and for taking care of my cells when I wasn't able to go to Casa Central. I would like to give a special thank you to Andrea Ramos for being such an integral part and being so supportive during this whole process. Without you I wouldn't have been able to get many of the results that I did. Thanks for keeping me sane and my hunger in check.

I would like to give a special thank you to my family and my boyfriend, Sebastian. Thank you for being so supportive every step of the way and for listening to my rants when I was so stressed. I love you all very much. And also my cat, Muffin, I know you can't read this, but thank you for staying up with me all of those nights and for keeping my lap warm while I typed.

TABLE OF CONTENTS

Pág.

LIST OF TABLES

Pg.

LIST OF FIGURES

NOMENCLATURE

C2C12	Mouse myoblast cell line
DAPI	4’,6-diamidino-2-phenylindole
DMEM	Dulbecco’s Modified Eagle medium
DSC	Differential scanning calorimetry
ECM	Extracellular matrix
FT-IR	Fourier transform infra red
MHC	Myosin heavy chain
PCL	Poly(ε-caprolactone)
PGA	Poly(glycolic acid)
PLA	Poly(lactic acid)
PLGA	Poly(lactic-co-glycolic acid)
poly(OTE)	Poly(octanoic acid 2-thiophen-3-yl-ethyl ester)
SEM	Scanning electron microscope
THF	Tetrahydrofuran
T_g	Glass transition temperature
T_m	Melting temperature

RESUMEN

El músculo esquelético tiene la capacidad de regenerar fibras musculares cuando se ha producido un daño, ya sea por lesiones o enfermedades degenerativas. Las células satélites son responsables de esta regeneración. Cuando se produce una lesión, estas células se activan y entran en el ciclo de proliferación para reparar el daño. Sin embargo, cuando el daño es demasiado extenso, no se puede producir la regeneración. *Scaffolds* de polímeros pueden ser usados para promover la diferenciación de mioblastos y así ayudar en la regeneración de tejidos. La respuesta de las células en los *scaffolds* de polímero se determina por factores tales como la composición de polímero, la topografía y la adición de otras moléculas como proteínas. La decorina, un proteoglicano que se encuentra en la matriz extracelular, aumenta la regeneración del tejido funcional y al mismo tiempo disminuye la fibrosis. Con el objetivo de estudiar el efecto de la morfología de fibras y la adición de decorina en ellas, sobre la respuesta celular del músculo esquelético, se evaluó la diferenciación de mioblastos murinos en fibras obtenidas mediante *electrospinning* (alineadas o no) de poli(ε-caprolactona) (PCL), y mezclas con poli(ácido láctico-co-glicólico) (PLGA) o decorina. Los resultados muestran que fibras alineadas de PCL con mayor contenido de PLGA favorecen el crecimiento celular, y mejoran la calidad de diferenciación en términos de largo, grosor y nucleación de miotubos. Al mismo tiempo, la presencia de decorina mejora en gran medida la cantidad y calidad de miotubos sobre las fibras, a pesar de que puede reducir su alineación. Esto sugiere que, a ciertas concentraciones, el efecto de la decorina sobre la diferenciación de mioblastos supera el efecto topográfico del alineamiento de las fibras. Por lo anterior, es fundamental optimizar simultáneamente la composición y topografía de un *scaffold* para poder ser usado en aplicaciones de regeneración muscular. Con este trabajo es posible preveer que una combinación de fibras alineadas de PCL/PLGA/decorina permitirá controlar efectivamente el crecimiento y la diferenciación de mioblastos en aplicaciones de ingeniería de tejidos.

Palabras Claves: *Electrospinning*, mioblastos, PCL, PLGA, decorina, *scaffolds*

ABSTRACT

Skeletal muscle has the ability to regenerate new muscle fibers when damage has occurred, be it from injury or degenerative diseases. Satellite cells are responsible for this regeneration. When injury occurs these cells are activated and enter the proliferation cycle to repair the damage. However, when the damage is too extensive, regeneration cannot occur. Polymer scaffolds can be used to promote differentiation of myoblasts to aid in tissue regeneration. Cell response on polymer scaffolds is determined by factors such as polymer composition, topography and the addition of other molecules. Decorin, a proteoglycan found in the extracellular matrix, has shown to increase the regeneration of functional tissue and simultaneously decrease fibrosis. We aimed to study the effect of fiber morphology and the addition of decorin on the response of skeletal muscle cells. We evaluated murine myoblast differentiation on unaligned and aligned fiber scaffolds composed of poly(ε-caprolactone) (PCL) and blends with poly(lactic-co-glycolic acid) (PLGA) and decorin. Aligned scaffolds that contained greater PLGA content had a greater cell count and greater differentiation yield, resulting in larger, more nucleated myotubes. The presence of decorin greatly improves the quantity and quality of myotubes on fiber scaffolds yet reduces myotube alignment. This suggests that at certain concentrations the effect that decorin has on myoblast differentiation trumps the topographical effect of fiber alignment. Considering this, it is essential to simultaneously optimize scaffold composition and topography for muscular regeneration. With this study, it is possible to foresee that a combination of aligned fibers composed of PCL/PLGA/decorin will allow effective control of the proliferation and differentiation of myoblasts applied to tissue engineering.

Keywords: Electrospinning, myoblasts, PCL, PLGA, decorin, scaffolds

1. INTRODUCTION

1.1 Skeletal muscle

Skeletal muscle tissue is one of the most abundant tissues of the body. It is a highly organized tissue with a hierarchal structure. It is composed of fiber-like structures called myofibers that are bundled together by a lipid layer bilayer, called sarcolemma, which contains collagen filaments and specialized proteins. These bundles form what is called a muscle fiber. Bundles of muscle fibers make up the muscle tissue (Lieber, 2002).

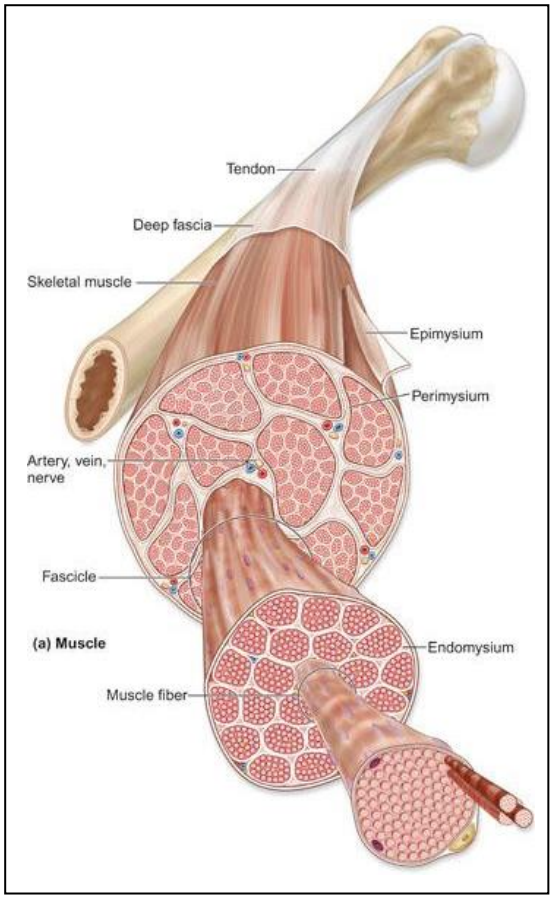

Figure 1-1: Skeletal muscle fiber structure (Mescher, 2016).

The synthesis of myofibers is produced by a process called myogenesis. Between the sarcolemma and the basal lamina are specialized muscle stem cells called satellite cells. These cells are responsible for muscle tissue regeneration. When the muscle has been injured, the previously quiescent satellite cells now activate and enter the proliferation cycle. Some of these cells remain satellite cells to maintain a steady population of stem cells while the others enter the proliferation cycle to become myoblasts (Olguin & Olwin, 2004). When the damage is too extensive, satellite cell population decreases and the tissue is incapable of regenerating resulting in permanent muscle loss.

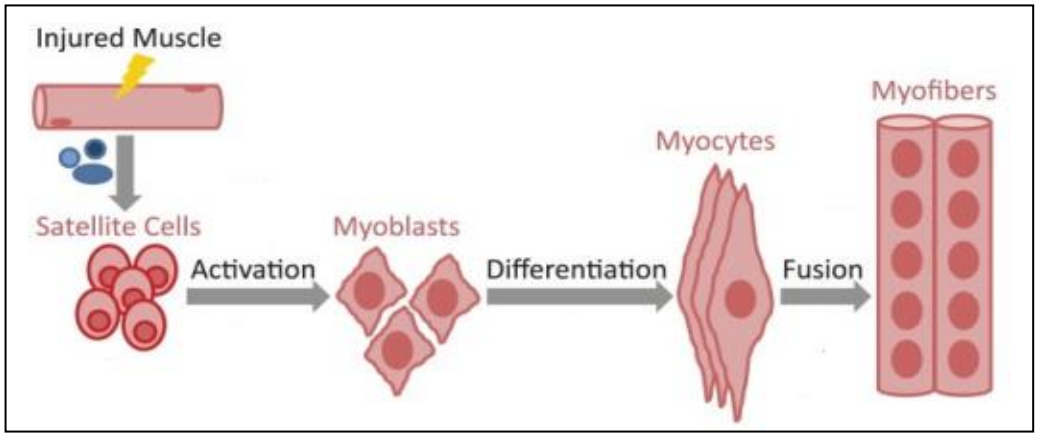

Figure 1-2: Myogenesis pathway (modified from Andres-Mateos et al. (2012))

1.2 Tissue engineering and scaffolds

Tissue failure as a result of injury or a genetic disease is a major health problem. Treatment options include transplantation (autologous or allogeneic), surgical repair, mechanical devices and drug therapy. However, major damage to the tissue can neither be repaired nor long-term recovery can be achieved in a truly satisfactory way with these methods. In the case of stem cell injection therapy, efficacy is low since cells can be systemically lost and therefore only a small

percentage of stem cells will remain in the affected area to carry out regeneration. Regarding skeletal muscle, microenvironment affects myoblast proliferation and differentiation. Damage tissue shrinks and becomes stiff. Satellite cells will sense this stiffness and proliferate but the resulting myoblasts will be stiffer than the original tissue, decreasing its functionality.

Tissue engineering is emerging as an alternative or a complementary solution. Tissue failure is treated by implanting substrates that are natural, synthetic, or a combination of both, which mimic the tissue microenvironment (i.e., extracellular matrix, ECM). These can be fully functional from the beginning or adapt to its environment to grow into the required functionality. The strategies used in tissue engineering can be classified into three groups:

1) Implantation of isolated cells or cell substitutes
2) Delivery of tissue-inducing substances (e.g., growth factors)
3) Placing cells on or within matrices

Scaffold design and fabrication are major areas of biomaterials research. Scaffolds are defined as three-dimensional porous yet solid biomaterials designed to perform certain functions. These functions can include some, if not all, of the following:

a) Promote interactions between cell and materials, cell adhesion and deposition of ECM
b) Allow the transport of nutrients, gases, and regulatory factors
c) Biodegrade in a controlled manner and at a rate which is similar to that of the regeneration of the tissue
d) Provoke little to no inflammation or toxicity (Langer & Tirrell, 2004).

1.3 Polymers used in tissue engineering

Biomaterials are defined as substances that have been engineered to interact with biological systems for a medical purpose (Ratner, 2004). A wide range of materials has been used as biomaterials, including – but not limited to – ceramics, metals, hydrogels and polymers. Polymers, both natural and synthetic, have been widely used as biomaterials for the fabrication of medical devices and tissue-engineered scaffolds (Piskin, 1994).

Natural polymers are biodegradable materials that have a biological origin. These can be classified as proteins (e.g., silk, collagen, gelatin, fibronectin, keratin), polysaccharides (e.g., cellulose, chitin, dextran), and polynucleotides (DNA and RNA) (Yannas, 2004). Thanks to its bioactive properties, natural polymers have better interactions with cells allowing them to enhance their performance.

Synthetic polymers are artificially-made materials. These polymers are highly used in the biomedical field since their properties (e.g., porosity, degradation rate, elasticity and tensile strength) can be customized for specific applications. Synthetic polymers tend to have a long shelf-life and can be produced in large quantities with high reproducibility under controlled conditions. Some of the most commonly used synthetic polymers for muscoskeletal tissue engineering include poly(caprolactone) (PCL), poly(L-lactic acid) (PLLA) and poly(lactic-co-glicolic acid) (PLGA).

1.3.1 Poly(caprolactone)

PCL is a hydrophobic, semicrystalline polymer; its crystallinity tends to decrease with increasing molecular weight. The good solubility of PCL, its low melting point (59-64 ºC) and exceptional blend-compatibility have stimulated extensive research into its potential application in the biomedical field (Nair & Laurencin, 2007). Due to the fact that PCL degrades at a slower rate than other synthetic polymers, it is used in drug delivery devices that remain active for over

one year and in slow degrading suture materials. However, PCL does not have the mechanical properties to be applied in high load bearing applications.

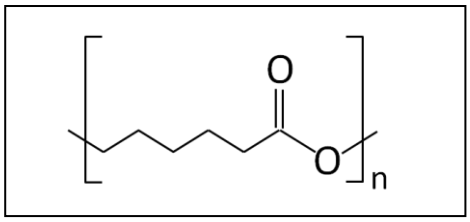

Figure 1-3: Chemical structure of poly(caprolactone).

1.3.2 Poly(lactic-co-glicolic acid)

PLGA, a polyester, is a copolymer of poly(lactic acid) PLA and poly(glycolic acid). PGA is void of any methyl side groups and shows highly crystalline structure in contrast to PLA (Figure 1-4). Presence of methyl side groups in PLA makes it more hydrophobic than PGA and therefore lactide-rich PLGA copolymers are less hydrophilic, absorb less water and in turn degrade more slowly. Mechanical strength, swelling behavior, and the capacity to undergo hydrolysis and therefore biodegradation rate of the polymer are directly influenced by the degree of crystallinity of the PLGA, which is dependent on the type and molar ratio of PLA to PGA. The glass transition temperature (T_g) of different copolymers of PLGA are reported to be above the physiological temperature of 37 °C and therefore are glassy in nature, exhibiting fairly rigid chain structure.

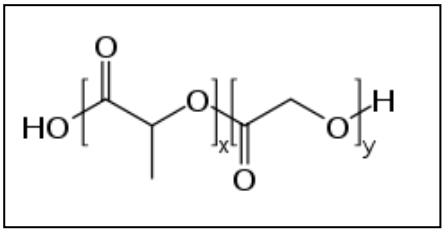

Figure 1-4: Chemical structure of PLGA, X corresponds to the number of lactic acid units and Y is the number of glycolic acid units.

1.4 Scaffold functionalization

Most of the synthetic polymers do not possess any specific functional groups, and they must be specifically functionalized for successful applications. The most popular and simplest scaffold modification methods are physical blending and coating. Polymers can be blended with other polymers, molecules such as proteins and growth factors and nanoparticles.

Bioactive molecules can promote engrafting by improving viability and survival of the engineered tissue. These molecules can be whole protein molecules such as ECM proteins. Many proteins have been used in scaffolds including collagen, gelatin, fibrinogen, albumin and decorin.

Decorin is a small leucine-rich proteoglycan, which is a component of the ECM of tissue that contains collagen (Hocking et al., 1998). This protein is important in regulating the correct assembly of collagen-containing matrices and controlling cell proliferation under many conditions. Decorin is regarded as an important modulator of matrix assembly, because of its ability to bind fibrillar collagen and delay in vitro fibrillogenesis (Giri et al., 1997; Noble et al., 1993). This proteoglycan can modulate the bioactivity of growth factors and act as a direct signaling molecule to different cells (Ständer et al., 1998). Decorin, which is expressed at high levels in skeletal muscle during early development (Nishimura et al., 2002) also interferes with muscle cell differentiation and migration and regulates connective tissue formation in skeletal muscle (Brandan et al. 1991).

Because differentiation is critical for skeletal muscle development and regeneration after injury and disease (Li et al., 2001), studies have examined the role of decorin in remodeling healing skeletal muscle. Li et al. (2007) showed that the direct injection of bovine decorin decreased muscle fibrosis and provided nearly complete functional recovery. Decorin blocks fibrosis, mostly by inhibiting transforming growth factor (TGF)-β activity, which improves muscle healing (Figure 1-5).

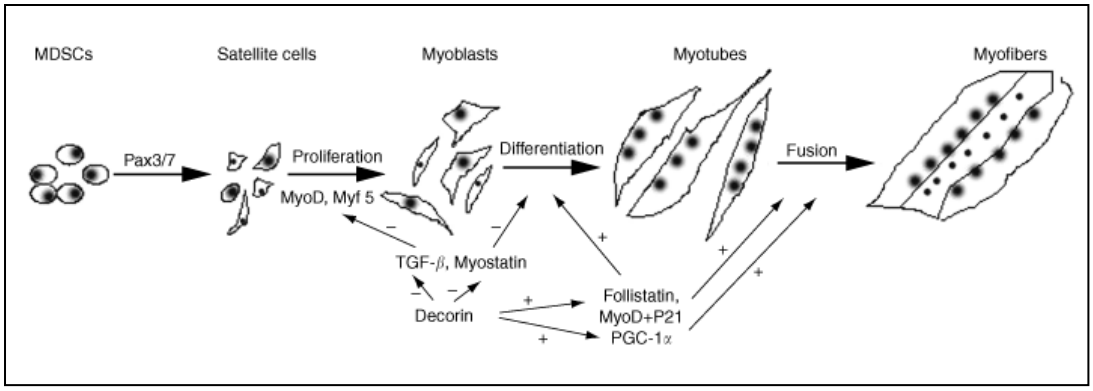

Figure 1-5: Schematic of the potential effect of decorin on muscle healing (Li et al., 2007).

Hinderer et al (2012) fabricated blended PCL/gelatin/decorin fiber scaffolds for tracheal tissue engineering applications. They found that decorin maintained its functionality and that those scaffolds had little immunogenicity.

1.5 Electrospinning

The development of nanofibers has enhanced the scope for fabricating scaffolds that can potentially mimic the architecture of skeletal muscle tissue at the nanometer scale. The high surface-area-to-volume ratio of the nanofibers combined with their microporous structure favors cell adhesion, proliferation, migration, and differentiation.

Electrospinning is a technique that uses high voltage to produce polymeric nanofibers. The basic setup (Figure 1-6) consists of four parts: a syringe with a metallic needle, a syringe pump, a metallic collector and a high voltage supply that is connected to the needle and the collector.

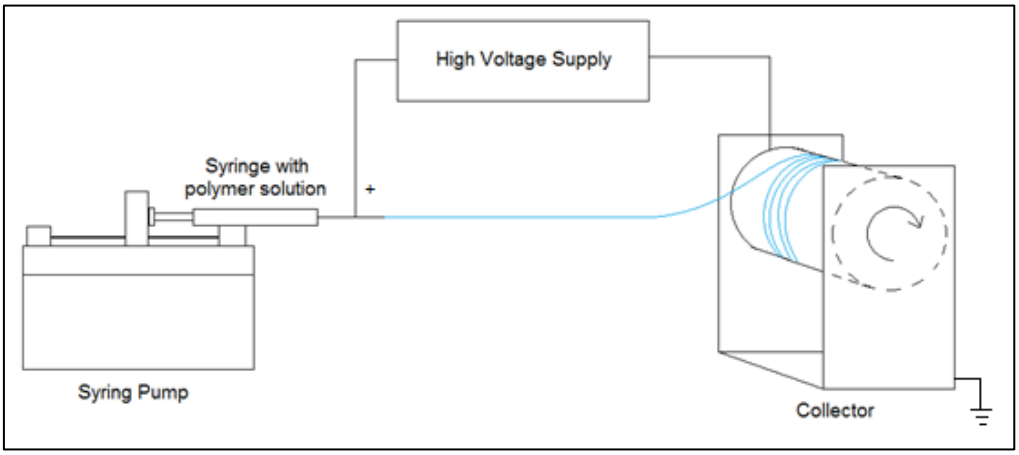

Figure 1-6: Schematic of electrospinning setup.

The process begins when electric charges move into the polymer solution through the metallic needle. This causes instability within the polymer solution as a result of the induction of charges on the polymer droplet. At the same time, the reciprocal repulsion of charges produces a force that opposes the surface tension, and as a result, the polymer solution flows in the direction of the electric field (i.e., towards the collector). A further increase in the electric field causes the spherical droplet to deform and assume a conical shape. The nanofibers emerge from the conical polymer droplet, called the Taylor cone, which are collected on the metallic collector. A stable charge jet can be formed only when the polymer solution has sufficient cohesive force. During the process, the internal and external charge forces cause the whipping of the liquid jet in the direction of the collector. This whipping motion allows the polymer chains within the solution to stretch and slide

past each other, which results in the creation of fibers with diameters small enough to be called nanofibers (Garg & Bowlin, 2011).

There are many factors that affect the electrospinning process that can be classified into three groups: electrospinning, solution, and environmental parameters. The electrospinning parameters include the applied electric field, distance between the needle and collector, flow rate, and needle diameter. The solution parameters include the solvent, polymer concentration, viscosity and solution conductivity. The environmental parameters include relative humidity and temperature. All of these parameters directly affect the generation of smooth and bead-free electrospun fibers (Matabola & Moutloali, 2013).

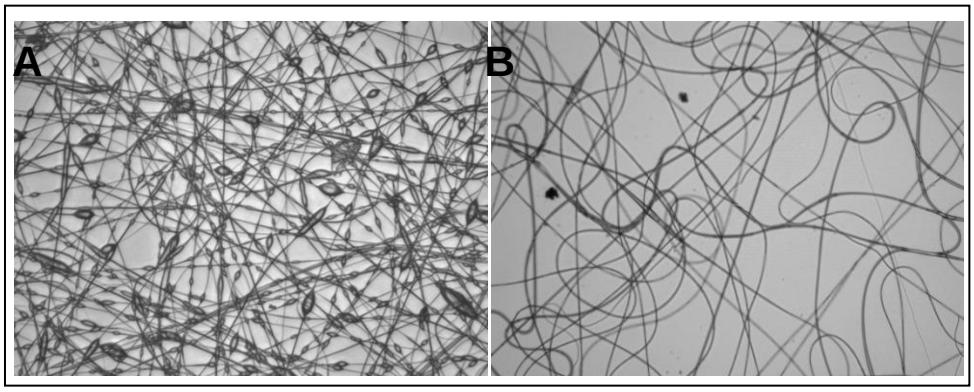

Figure 1-7: Transmitted light microscopy micrographs of electrospun 15% w/v PLGA fibers in tetrahydrofuran (THF) at 15 kV, 15 cm distance needletip-collector A) flow rate 0.5 mL/h and 60 min collection time (with beads) B) flow rate 0.3 mL/h and 40 min collection time (without beads) (magnification 20X).

An increase in the applied voltage beyond the critical value will result in the decrease in fiber diameter and increase in the formation of beads. The decrease in diameter is because the stretching of the polymer solution is correlated with the charge repulsion within the polymer jet. Both of these effects are attributed to the

decrease in the size of the Taylor cone and increase in the jet velocity for the same flow rate (Deitzel et al., 2001).

The distance between the needle and collector affects the porosity and spread of the nanofibers. By increasing the distance, the nanofibers have more space to whip back and forth more, causing a larger spread in nanofibers that deposit on the collector. This increased spread also translates into an increase in the overall "porosity" of the scaffold (i.e., space between the fibers). When the distance is decreased, the scaffold porosity is decreased and bead formation is increased. The decrease distance also decreases deposition time, which means that the solvent does not have enough time to evaporate completely. The excess solvent manifests in the formation of polymer beads (Matabola & Moutloali, 2013).

Flow rate of the polymer solution determines the morphology of the fibers. An increase in flow rate produces beads and ribbon-like structures. This is mainly due to the lack of evaporation of the solvent and the low stretching of the solution in flight. This also explains the increase in fiber diameter with increase in flow rate (Megelski et al., 2002).

The electrospinning process relies on the phenomenon of the longitudinal stretching of a charged jet. This stretching is significantly affected by changing the concentration of the polymeric solution. When the concentration of the polymeric solution is low, the applied electric field and surface tension cause the entangled polymer chains to break into fragments before reaching the collector (Haider et al., 2013). These fragments cause the formation of beads or beaded nanofibers. Increasing the concentration of the polymer solution leads to an increase in the viscosity, which increases the chain entanglement among the polymer chains. These entanglements overcome the surface tension and result in uniform nanofibers with no beads. This happens at critical concentration of polymer solution. Further increasing the concentration beyond the critical value hinders the flow of the solution through the needle tip. The little solvent in the solution evaporates quickly

and the solution dries at the tip of the needle, causing blockage, resulting in the formation of beads.

Humidity and temperature are also important factors that influence the electrospinning process. An increase in environmental humidity lowers the evaporation of the solvent leading to the increase in the formation of beads on the nanofibers. The same occurs with a decrease in the temperature of the environment. Humidity has also shown to affect the porosity and the diameter of the nanofibers. Increased humidity increases the porosity of the individual fibers.

The type of collector affects the alignment of the nanofibers. A metal plate is the simplest collector that is used. This collector produces unaligned fibers. A rotating cylinder can produce highly aligned fibers (Figure 1-8). At high speeds (around 1500 rpm), aligned fibers can be obtained. Low speeds produce unaligned fibers.

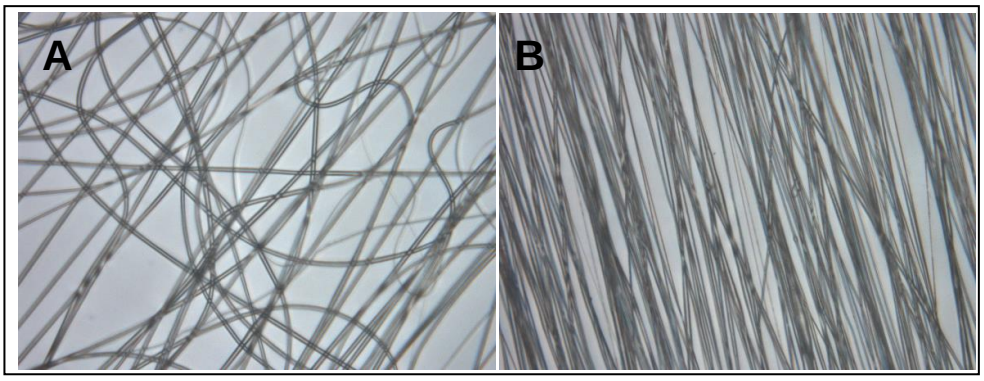

Figure 1-8: Transmitted light microscopy micrographs of polymer fibers made of PCL in chloroform electrospun at 12 kV, 0.3 mL/h, 18cm distance, for 2 hours, producing A) unaligned (200rpm) and B) aligned (2000 rpm) fibers (magnification 40X).

1.6 Document structure

This document is divided into the following sections. Section 2 states the hypothesis and objectives that we defined for this study. Section 3 contains the paper that was submitted to Journal of Biomedical Material Research Part A. Section 4 contains additional results and further discussion and conclusions. Section 5 contains annexed information.

2. HYPOTHESIS

The hypothesis of this work is that the alignment of PCL-based fiber scaffolds and the addition of other bioactive compounds improve murine myoblast differentiation.

2.1 Objectives

The objectives of this study include the following:

a) Evaluate myoblast differentiation on different fiber morphologies

   i) Evaluate myoblast differentiation on unaligned and aligned PCL and PCL/PLGA fiber scaffolds

   ii) Evaluate myoblast differentiation on PCL and PCL/PLGA fibers of different diameters

b) Evaluate myoblast differentiation on different polymer blends

   i) Evaluate myoblast differentiation on PCL and PCL/PLGA fiber scaffolds

   ii) Evaluate myoblast differentiation on aligned PCL fibers with the addition of decorin

3. IMPROVING MYOBLAST DIFFERENTIATION ON ELECTROSPUN POLY(E-CAPROLACTONE) SCAFFOLDS

Phammela N. Abarzúa-Illanes[1], Cristina Padilla[1], Andrea Ramos[1], Mauricio Isaacs[2,3], Jorge Ramos-Grez[3,4], Hugo C. Olguín[5*], Loreto M. Valenzuela[1,3*]

[1]Department of Chemical and Bioprocess Engineering, School of Engineering, Pontificia Universidad Católica de Chile, Santiago, Chile.

[2]Department of Inorganic Chemistry School of Chemistry, Pontificia Universidad Católica de Chile, Santiago, Chile.

[3]Research Center for Nanotechnology and Advanced Materials "Cien-UC", Pontificia Universidad Católica de Chile, Santiago, Chile.

[4]Mechanical and Metallurgical Engineering Department, Pontificia Universidad Católica de Chile, Santiago, Chile.

[5]Department of Cellular and Molecular Biology, School of Biological Sciences, Pontificia Universidad Católica de Chile, Santiago, Chile.

*corresponding authors: holguin@uc.cl; lvalenzr@ing.puc.cl

3.1 Abstract

Polymer scaffolds are used as an alternative to support tissue regeneration when it does not occur on its own. Cell response on polymer scaffolds is determined by factors such as polymer composition, topology, and the presence of other molecules. We evaluated the cellular response of murine skeletal muscle myoblasts on aligned or unaligned fibers obtained by electrospinning poly(ε-caprolactone) (PCL), and blends with poly(lactic-co-glycolic acid) (PLGA) or decorin, a proteoglycan known to regulate myogenesis. The results showed that aligned PCL fibers with higher content of PLGA promote cell growth and improve the quality of differentiation in terms of cell fusion, myotube length and thickness. At the same time, the addition of decorin greatly improves the quantity and quality of differentiated cells. Interestingly, our results suggest that at certain concentrations, the effect of decorin on myoblast differentiation exceeds the topological effect of fiber alignment.

Keywords: muscle regeneration, electrospinning, myoblasts, PCL, PLGA, decorin

3.2 Introduction

Skeletal muscle is a highly organized tissue composed of bundles of muscle cells called myofibers. These myofibers are formed when myoblasts differentiate and fuse with one another. Located between the myofiber's plasma membrane and the surrounding basal lamina, are the satellite cells. These muscle specific stem cells activate upon different stimuli such as myofiber damage for tissue regeneration and maintenance (Olguin & Olwin, 2004).

When a large portion of the muscle has been affected, satellite cells are incapable of fully recovering the tissue (Karalaki et al., 2009). By using polymer scaffolds as a structural and functional platform for cells, skeletal muscle can be regenerated *in vitro* and then implanted into the patient when the tissue is sufficiently mature.[3]

Skeletal muscle cells have been grown *in vitro* on many scaffold materials including natural and synthetic polymers. These include collagen, poly(L-lactic acid) (PLLA) and poly(D-lactic acid) (PDLA). Although collagen is widely used, its drawbacks include poor mechanical properties and a rapid degradation rate. Polymers with increased mechanical properties are necessary to be able to withstand the tensile load of muscular contractions. For example, poly(ε-caprolactone) (PCL) has been used for medical devices because its biocompatibility, flexibility, stability and low cost (Tang et al., 2005) It has a slow degradation rate (around 24 months), is hydrophobic and therefore has no physiological active sites, i.e., it lacks surface recognition functions for specific mucoadhesion or receptor recognition (Ciardelli et al., 2005). Other polymers such as poly(lactic-co-glycolic acid) (PLGA) are also biocompatible, exhibit higher degradation rates (e.g., 4-5 weeks for PLGA 75/25) and have good cellular response because of their hydrophilic properties (Gentile et al., 2014; Kim & Cho, 2009).

Adding bioactive molecules to scaffolds can enhance cellular response by imitating the extracellular matrix. Decorin, a leucine rich proteoglycan found in the muscle extracellular matrix, improves muscle regeneration and decreases fibrosis

(Li et al., 2007), by upregulating factors such as follistatin (promotor of differentiation and fusion of myotubes), downregulating myostatin expression (inhibitor of myogenesis) (Amthor et al., 2004), and regulating transforming growth factor (TGF-β) which controls myoblast differentiation (Chen et al., 2016; Li et al., 2006; Sartori et al., 2014).

Electrospun scaffolds provide an extracellular matrix (ECM)-like substrate – mimicking tissue organization and architecture – to which cells can adhere to before secreting their own ECM. Therefore, aligned fiber scaffolds are most suitable for skeletal muscle tissue engineering. Stem cells use scaffold topology information to repair muscle tissue *in vivo* (Meng et al., 2014; Webster et al., 2016), where scaffold alignment aids in cell proliferation (Whited & Rylander, 2014). Huang et al.(2006) cultured C2C12 myoblasts on electrospun PLLA fibers and found that the myotubes that were produced were highly organized growing along the nanofibers. Choi et al. [17] showed similar results with human skeletal muscle cell grown on PCL/collagen fibers.

With the objective of simultaneously evaluate the effect of alignment and fiber composition on myoblast response, we compared myoblast proliferation and differentiation on electrospun fibers, aligned or not, and blends of PCL/PLGA and PCL/decorin.

3.3 Materials and methods

3.3.1 Polymer fiber preparation

PCL (Mn = 70 – 90 kDa), PLGA 75:25 (Mn = 66 – 107 kDa), chloroform, and decorin bovine articular cartilage were purchased from Sigma-Aldrich. 15% w/v and 20% w/v solutions of PCL and PLGA in chloroform were prepared by continuous stirring for 1 hour. These in turn were used to prepare solutions of PCL and PCL blended with 25% or 50% in mass of PLGA.

Each of the aforementioned solutions was loaded in a 1 mL glass Hamilton syringe with a 21 G blunt tip needle and electrospun using a high voltage DC power supply set between 12 - 25 kV from a distance of 18 - 18.5 cm (distance needle-tip to collector). The syringe pump was operated at a flow rate of 0.3 mL/h. The collector used was a copper covered solid stainless steel rotating cylinder of a diameter of 2 in. Coverslips that were previously dipped in 2% w/v polymeric solution with the same composition as the fibers were placed on the collector surface. The collector was rotated for 3 h at 200 rpm to produce randomly aligned fibers and at 2000 rpm to produce aligned ones.

Additionally, PCL was mixed with 50 μg/mL decorin and electrospun with the same aforementioned parameters, or 400 μL of 50 μg/mL decorin was added to PCL fibers for 1 h following protocol used by Leach et al. (2011), while untreated PCL fibers were used as control.

Before cell seeding, coverslips were sterilized under a laminar flow hood with successive 30 minute washes with the following solutions: 70% ethanol, 50% ethanol, 25% ethanol, distilled water, according to Li and Tuan (2009).

3.3.2 Cell culture

Stock C2C12 (ATCC CRL-1772) cells were detached from the plate by enzymatic digestion with trypsin and centrifuged at 1000 rpm at 19 °C for 5 minutes as previously reported by Olguín and Olwin (2004). Cells were resuspended and counted using a Neubauer chamber. Wells with scaffolds were subsequently plated at 2,500 cells/cm^2 or 12,000 cells/cm^2 for proliferation and differentiation conditions, respectively. Cells were cultured in DMEM (Life Technologies) and 10% fetal bovine serum (Hyclone) (proliferation medium) at 37 °C and 5% CO_2. After 48 h of incubation, cells were induced to differentiate in DMEM with 5% horse serum (Hyclone) and were incubated for 4 more days. After 5 and 7 days of incubation for proliferation and differentiation cultures respectively, cells were fixed with paraformaldehyde (PFA) 4% in PBS for 20 min, permeabilized with PBS

+ 0.2% triton X-100 for 20 min at room temperature and stained with haemotoxylin-eosin (Padilla et al., 2016). Each sample was divided into 5 quadrants and one field was photographed from each quadrant using an Olympus microscope (model CKX41SF) with a MEM 1300 camera. ImageJ software and DiameterJ plugin was used to measure percentage area of cell spreading and aspect ratio.

3.3.3 Myogenin and myosin heavy chain expression

C2C12 cells were maintained in differentiation medium for 9 days (for a total incubation period of 12 days). Scaffolds with cells were fixed with paraformaldehyde 4% in PBS for 1 min, and were later permeabilized with PBS, 0.5% Triton-X100 for 5 min. Non-specific binding sites were blocked with PBS, 3% BSA. Primary antibodies rabbit polyclonal anti-myogenin (1:200) and mouse monoclonal anti-MHC (1:250) (Developmental Studies Hybridoma Bank) were incubated for 2.5 h. Secondary antibodies donkey anti-rabbit (A31572, Alexa Fluor 555, Life Technologies Corporation) and donkey anti-mouse (A21202, Alexa Fluor 488, Life Technologies Corporation) diluted at 1:500 each were incubated at room temperature for 1.5 h. Cells were mounted with VECTASHIELD mounting medium containing DAPI (Vector Laboratories). Each sample was divided into 9 quadrants and one field was photographed from each quadrant using a MoticBA410 microscope equipped with a Moticam Pro 252B camera. Images were processed with ImageJ (Schneider et al., 2012), measuring the aspect ratio (ratio between the length and width of each myotube), which is an indicator of myotube thickness (Ren et al., 2008), fusion index: the percentage of total nuclei that are found within the myotubes; considering myotubes with > 2 nuclei (Ren et al., 2008), number of nuclei per myotube, and nuclei orientation. Measurements of each quadrant were taken and later averaged.

3.3.4 Scaffold characterization

Scaffolds were observed under an inverted optical microscope (Olympus model CKX41SF) with a MEM 1300 camera. Fiber diameter was measured using Q-capture Pro 7. ImageJ software with plugin DiameterJ was used to measure fiber radius, angle of orientation, and porosity (Hotaling et al., 2015). Kurtosis for angle of orientation graphs was measured in Excel. Kurtosis is a measure of "tailedness" of the probability distribution of a real-valued random variable. Positive kurtosis indicates heavy tails while negative values indicate light tails (Westfall, 2015).

a) Scanning Electron Microscope (SEM)

Electrospun scaffolds were analyzed using a SEM (FEI Inspect F50) at 1000X. Samples were mounted onto stubs and coated with gold using Sputter Coater 108 auto (Cressington). Fiber diameter was measured at 24,000X magnification. Average fiber diameter and pore sizes were analyzed with ImageJ software.

b) Differential Scanning Calorimetry (DSC)

Differential Scanning Calorimetry (DSC) was used to chemically characterize the fibers for melting temperature (T_m) and glass transition temperature (T_g), using DSC 6000 (Perkin Elmer) with Pyris Software. The heating rate was 10 °C/min under nitrogen atmosphere with a heating temperature range between -80 °C to 200 °C for 2 cycles.

c) Fourier transform infrared microscopy (FT-IR)

Films of PCL, PLGA, and PCL/PLGA blends with 25 and 50 % of PLGA were prepared by solvent casting with chloroform as the solvent for analysis. The samples were analyzed with Fourier transform infrared spectroscopy (FT-IR) using a Vector 22 spectrometer. Spectra were collected between a wavelength of 400 and 4000 cm^{-}

[1] with 32 scans. OPUS software was used to control the spectrometer and obtain and analyze the spectra.

3.4 Results

3.4.1 Differential Scanning Calorimetry

T_g and T_m of PCL films were -61.36 °C and 57.56 °C, respectively. Both temperatures were found in both PCL/PLGA blends (Figure 3-1). T_g and T_m for PLGA could not be obtained from the DSC measurements because its T_g is in the same range of the T_m of PCL (as reported by Sigma-Aldrich, Table 3-1) and its T_m is higher than 100 °C, temperature that was not passed to avoid thermal decomposition of the polymers (as reported by Sigma-Aldrich, Table 3-1).

3.4.2 Fourier Transform Infrared Spectroscopy

PCL FT-IR spectrum showed characteristic signals from the carbonyl group (C=O) found in esters at 1724 cm^{-1}, C-H aliphatic asymmetric and symmetric stretching at 2944 and 2862 cm^{-1}, C-O and C-C stretching at 1294 and 1046 cm^{-1}, and C-O-C asymmetrical and symmetrical stretching at 1242 and 1165cm^{-1}, respectively. PLGA spectrum showed signals at 1757 cm^{-1} for C-O stretching from carbonyl groups, aliphatic C-H asymmetrical and symmetrical stretching at 2991 cm^{-1} and 2936 cm^{-1}, C-O stretching at 1130cm^{-1}, and C-O-C symmetrical stretching at 1185cm^{-1} (Figure 3-2). The spectra of both blends of PCL/PLGA show all of the corresponding bands from both of the polymers comprising the mixture (Figure 3-2).

3.4.3 Fiber morphology

Analysis of transmitted light microscopy images indicated that unaligned fibers are oriented in many directions while aligned fibers are generally parallel (Figure 3-3, Figure 3-4 and Table 3-2). There is no significant difference in scaffold

porosity within the studied scaffolds: 60.6 ± 8.5% and 60.4 ± 9.7% for unaligned and aligned fibers, respectively (Figure 3-5).

3.4.4 Scanning Electron Microscopy

SEM images of fiber scaffolds corroborate the alignment that was observed with the microscope images (Figure 3-6 and Figure 3-3, respectively). Average fiber diameter ranges from 0.8 – 1.1 μm to 1.0 – 3.2 μm for unaligned fibers, made from 15% w/v and 20% w/v of polymer solution, respectively. Aligned fiber diameter ranges from 0.4 – 0.7 μm to 0.7 – 2.7 μm, for 15% w/v and 20% w/v of polymer solution, respectively (Figure 3-7).

3.4.5 Cell proliferation

Myoblasts on aligned fibers are more elongated and cover less area per cell (Figure 3-8 and Figure 3-9). Scaffolds with 50% of PLGA content and 20% w/v polymer contain the greatest number of myoblasts of the studied fibers; there are no significant differences with these scaffolds and the control (Figure 3-9). Myoblasts follow the general direction of fiber alignment; i.e., the major axis of myoblast nuclei extends parallel to the fibers (Figure 3-10 and Table 3-3). Cells that were seeded on unaligned fibers had nuclei with a wide distribution of different orientation, as shown with its negative kurtosis values.

3.4.6 Cell differentiation

The myotubes that were present on the fibers with 50% PLGA were as thick as the previous scaffolds but were much longer and had numerous nuclei (< 10) (Figure 3-11). PCL fibers with 50% PLGA reached a high confluence (> 86%) by the end of the incubation period (7 days) and had the greatest amount of myotubes (> 7% of area covered by myotubes) (Figure 3-12). Higher concentration of PLGA increased the aspect ratio of myotubes. Myotubes on PCL fiber scaffolds were short and very thin, and generally had no more than 5 nuclei. Myotubes on PCL/25%

PLGA had similar lengths but were much thicker and had more than 3 nuclei. There were no significant differences in aspect ratio between the control and PCL/5% PLGA fibers (Figure 3-13).

3.4.7 Decorin addition

In presence of decorin, the myotubes formed were at least 10% larger (p-value=0.065) and 51% thicker (p-value=0.00081), and the fusion index was at least 71% higher (p-value=0.047) than without decorin (Figure 3-14 and Figure 3-15). Furthermore, when decorin was blended in the polymer solution, the myotubes were more numerous, with more than twice the number of myotubes (p-value=0.0022) than with the decorin coating, and the fusion index was three times higher than the control (p-value=0.0039). Myotubes that formed in the presence of decorin expressed more MHC than without it. PCL fibers expressed more myogenin, an early differentiation marker, and very little MHC, a late differentiation marker (Andres & Walsh, 1996). Nuclei maintained unidirectional alignment on the control and on fibers with coated decorin (kurtosis = 0.493 and 0.271, respectively). When decorin was blended, nuclei were less aligned (kurtosis = -0.351) (Figure 3-16).

3.5 Discussion

Polymer scaffolds support cell growth and differentiation. They can also support stem cell function and/or delivery, and therefore constitute a powerful tool for regenerative medicine. Here we evaluated the cellular response of murine skeletal muscle myoblasts on aligned or unaligned fibers obtained by electrospinning PCL and blends with PLGA or the proteoglycan decorin.

As expected, FTIR measurements are in accordance to those found in literature (Elzein et al., 2004; Nourmohammadi et al., 2016). The spectra of PCL and PLGA, both aliphatic poliesters, show the characteristic peaks, especially C-O-C, C-C and C=O bands, that make up the main chain and the carbonyl group (Figure 3-2). The peak corresponing to the -OH terminal group in PLGA that

should be in the high wavenumber region (approximately 3600 cm^{-1}) (Fisher, 2007; Rodriguez et al., 2014) is not observed in our samples, probably due to the small proportion of end groups in a large molecular weight polymer (less than one end group per 1000 monomer units). No new bands are present, indicating that the mixture is a result of the physical interactions between the polymers (Hiep & Lee, 2010; Kemala et al., 2012).

Lower fiber diameter of aligned fibers is due to the mechanical forces that act upon the polymer jet stream as it comes into contact with the rotating collector. At high rotational speeds the diameter of the fibers decreases because of stretching (Haider et al., 2013). Aligned fibers are uniform due to the relatively constant stretching produced by a constant rotational velocity. High rotational speeds do not give fibers enough time to deposit more polymer solution, which can produce beads and/or thicker fibers. Additionally, scaffold porosity was not significantly different among the samples studied, thus it was not concluded as a relevant factor on this study.

Larger diameter fibers promote myoblast proliferation. Thicker polymer fibers offer a better topological guidance cue for myoblasts since they are more protuberant (Langhammer et al., 2013). Both diameter and composition are important factors that control the mechanical properties of the fibrous scaffolds (Li et al., 2006; Tan et al., 2005), which influence myoblast proliferation. Thicker fibers imply higher stiffness (Baumgart & Cordey, 2001; Markaki & Clyne, 2003). Thicker fibers provide a larger contact area for the cells per fiber and therefore they promote myoblast proliferation.

On the other hand, thinner fibers promote myoblast differentiation. It has been reported that substrate stiffness affects skeletal myoblast differentiation (Romanazzo et al., 2012). Myoblasts differentiate optimally on softer substrates with tissue-like stiffness (Engler et al., 2004). The thinner fibers are less structurally stiff and therefore more similar to tissue stiffness (elastic modulus of muscle tissue ~ 5-15 kPa (Fung, 1993)) than the thicker fibers. However, our

results also show that myotubes are able to develop on stiffer fibers, i.e., those with higher PLGA content.

Aligned fibers presented a greater number of and more aligned myotubes compared to unaligned fibers. Cell-to-cell contact is vital for differentiation to myotubes (Romanazzo et al., 2012). High confluence increases the probability of cells finding neighboring cells, which facilitates faster and greater cell fusion, which is observed in the aligned fibers. Myoblasts on aligned fibers are more stretched, which helps them to reach neighboring cells. Myoblasts that are parallel to each other have more contact points, facilitating cell-to-cell contact, which is important for fusion (Chen et al., 2007).

Myoblast proliferation on electrospun PCL fibers is improved by the addition of PLGA in the blend. PCL is an elastic polymer but has no physiological active sites (Ciardelli et al., 2005), while PLGA is a stiffer polymer that has hydrophilic properties and physiological active sites (Kim & Cho, 2009) which have a positive impact in cellular response; myoblast proliferation is increased on fibers with higher PLGA content.

As expected, stiffer substrates including blends with 50% PLGA content, thicker fibers and glass coverslips displayed the highest myoblast proliferation [41]. Engler et al. (2004) found that cell adhesion strength increases as substrate stiffness increases. According to Trensz et al. (2015), microenvironment stiffness is a stress signal for myoblasts which causes increased proliferation by increasing the amount of satellite cells that activate into myoblasts. However, stiffer environments will also produce stiffer and tenser cells, decreasing their functionality (Engler et al., 2006), and increasing fibrosis. Further studies should be carried out to optimize PLGA concentration to be able to increase myoblast proliferation yet regulate stiffness to simulate muscle tissue (E ~ 5-15 kPa) (Fung, 1993). Engler et al.(Engler et al., 2004) showed that only when substrate stiffness is similar to tissue stiffness myotube, striations (i.e., sarcomere) can be observed, which are characteristic of maturation to skeletal muscle fibers.

The addition of PLGA also improves the quality of differentiation. Although PCL fibers displayed a high aspect ratio, these myotubes were not as long as those present on PLGA fibers, and therefore were much thinner. The longer, thicker and more nucleated the myotube, the better its quality, improving muscle fiber assembly. Since myofibers have diameters that measure up to a few hundred micrometers and lengths that range from a few millimeters to centimeters (Burkitt et al., 1995; Junqueira & Carneiro, 1995), the thicker and longer the myotube, the greater similarity it will have with *in vivo* myofibers.

Decorin has a positive impact on myoblast differentiation (Figure 3-15). We observed 57% (p-value=0.0008) less myotubes form on PCL fiber scaffolds without decorin. This could be related to diminished cell proliferation or migration, both regulated by decorin (Olguin & Brandan, 2002; Romanazzo et al., 2012). This in turn affects the formation of myotubes causing less and thinner myotubes to be present in PCL scaffolds. With decorin, there is a greater number of myotubes present in scaffolds, which are much thicker, longer and have more nuclei than the PCL scaffolds without decorin.

PCL fibers with decorin within the solution exhibited myotubes with significantly increased number of nuclei that expressed more MHC than the other scaffolds (Figure 3-14). This indicates that scaffolds with decorin in the solution enhance muscle-specific gene expression, favoring differentiation and myotube formation, as described by Li et al. (2007). The addition of decorin in the polymer solution significantly increases the number of nuclei within the myotubes. Myotubes are able to reach more mature stages of differentiation by fusing and form even larger myotubes. These results suggest that the addition of decorin can greatly improve myoblast differentiation even on poor polymer scaffolds such as PCL.

It is worth noting that scaffolds with decorin directly incorporated into the polymeric solution have a better quality (i.e., longer, more nucleated, and greater number) of myotubes than those that were just dipped in decorin. This is

presumably because the dipped scaffolds had the protein only adsorbed on the surface via weak interactions such as van der Waals. Therefore, it is possible to speculate that upon ethanol washes, some of the decorin was washed away.

Although decorin has positive effects on myoblast proliferation and differentiation, increasing amounts of this protein negatively affect cell alignment (Figure 3-16). Seemingly, there is a tradeoff between myoblast proliferation and alignment. Given the greater amount of decorin present within the fiber (prepared in the solution), the signal of this protein is much greater than the topological signal from the fiber itself. Therefore, the cell will be attracted more to the location of the protein then the orientation of the fiber. This allows myoblasts to ignore the direction of the fiber, since the chemical cue is stronger than the physical (topological) cue, which has been observed before by Abdellatef et al. (2014).

3.6 Conclusions

Both physical and chemical properties of polymer scaffolds determine myoblast proliferation and differentiation. Larger diameter fibers promote myoblast proliferation but less differentiation. Fiber alignment promotes a greater number of and more aligned myotubes. Both of these observations may be related to fiber stiffness that depends on diameter and alignment.

The addition of PLGA on PCL blends greatly improves cell proliferation and differentiation. PLGA is very biocompatible in terms of myoblasts because it is hydrophilic and has physiological active sites. In addition, PLGA's high stiffness can trigger increased myoblast proliferation but also increases cell stress and stiffness. Furthermore, the addition of decorin greatly improves the quality and quantity of myoblast differentiation. While decorin has a positive effect on myoblast growth, there is a tradeoff with cell alignment, which should be optimized in future research. PCL/PLGA/decorin fiber scaffolds could be suitable to produce highly differentiated and mature myotubes. These findings could be used to improve scaffold fabrication to be able to culture more mature muscle tissue *in vitro*.

Future work includes studies to optimize PLGA content to increase myoblast proliferation and maintain cell stiffness similar to that of skeletal muscle. Therefore, myoblasts could be cultured and matured *in vitro* to then be implanted into the affected area without stressing the new regenerative cells with stiff, damaged tissue.

3.7 Acknowledgments

We want to thank all the members from Dr. Olguin's and Dr. Valenzuela's laboratories for insightful discussions and suggestions. This work was supported by the interdisciplinary grant VRI 43/2011 from Pontificia Universidad Católica de Chile, CONICYT (FONDECYT 11121392 and 11130631), and Ministerio de Economía, Fomento y Turismo, Chile (Project RC 130006, CILIS, granted by Fondo de Innovación para la Competitividad).

3.8 Figures

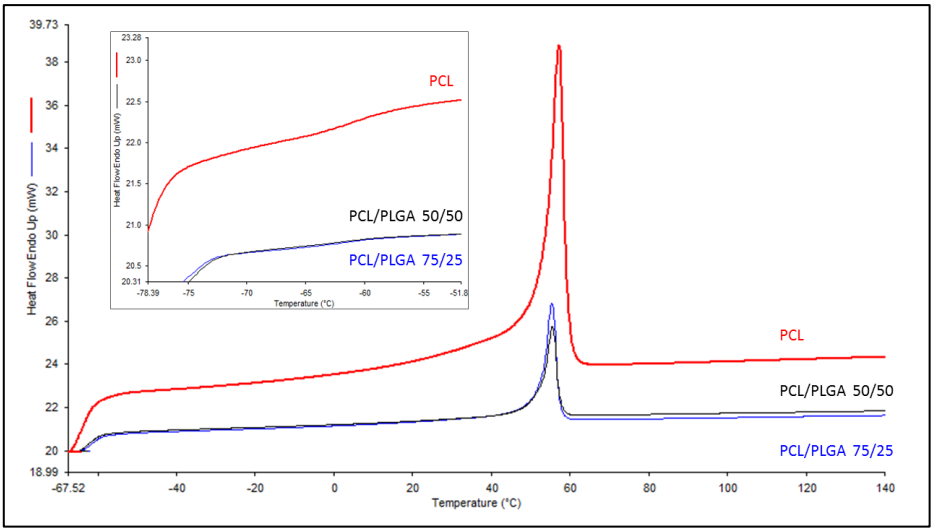

Figure 3-1: Thermograms for PCL and PCL/PLGA blends (75/25 and 50/50). Scaffolds were heated at a rate of 10°C/min between a range of -70°C and 150°C. Zoom shows glass transition (inset).

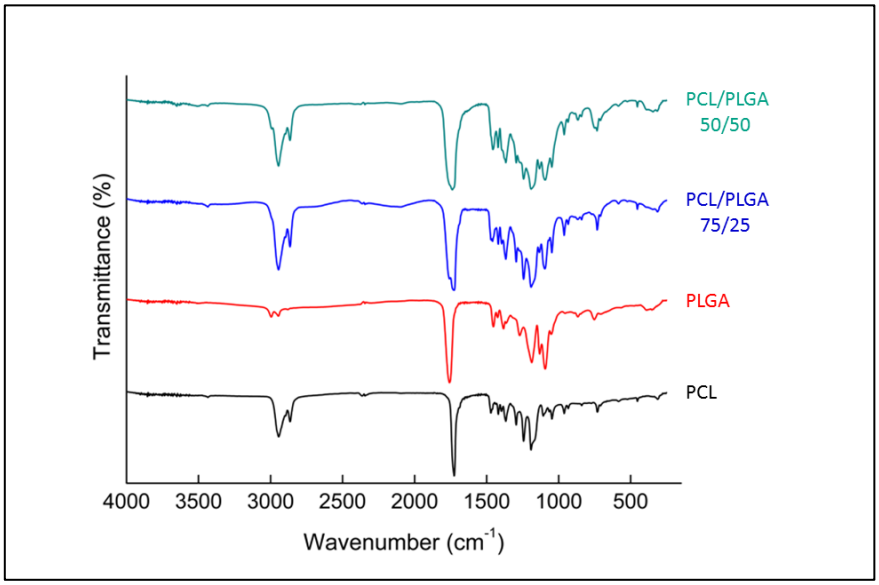

Figure 3-2: FT-IR spectra of PCL, PLGA and PCL/PLGA blends.

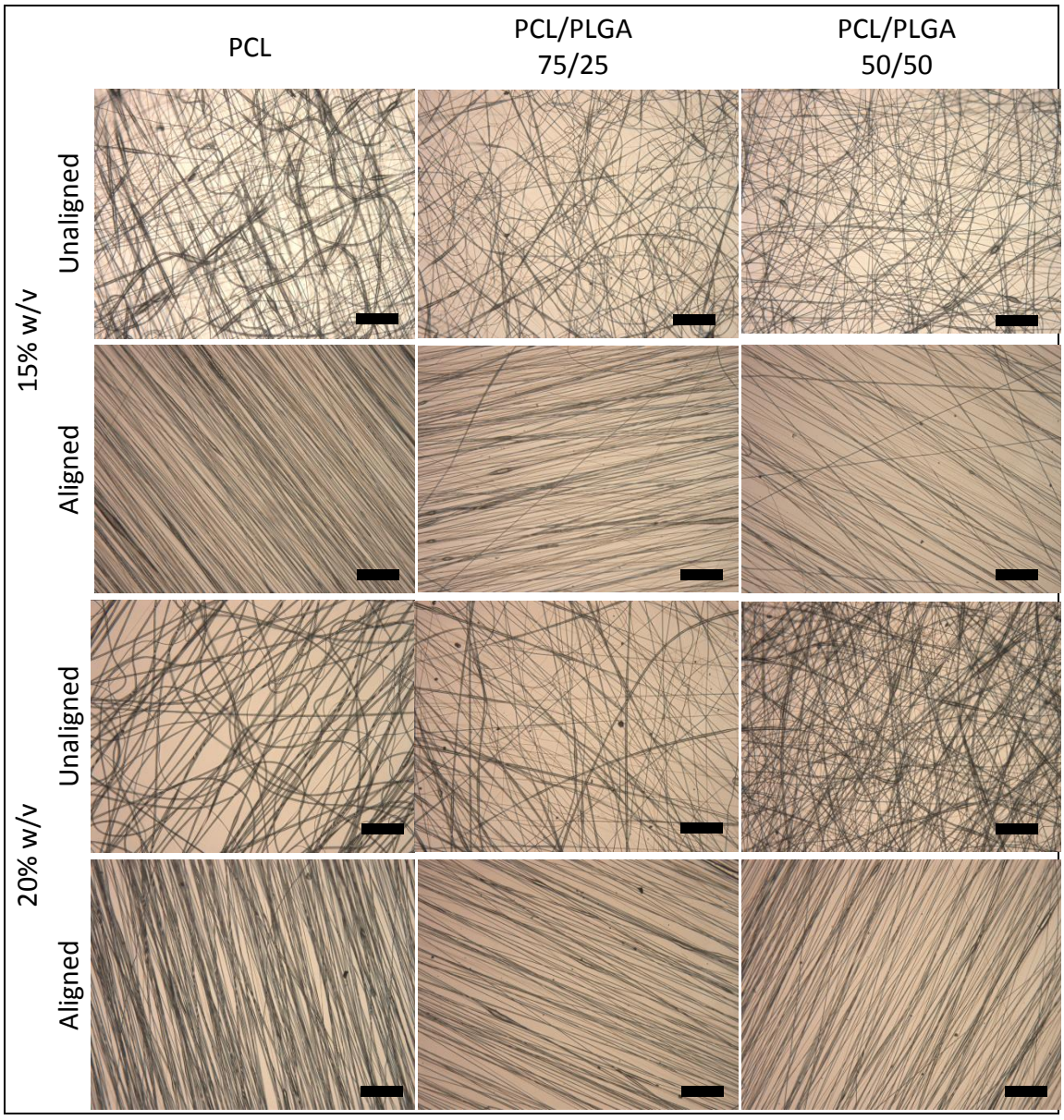

Figure 3-3: Transmitted light microscopy micrographs of aligned and unaligned electrospun scaffolds of PCL and PCL/PLGA blends prepared in 15% and 20% w/v concentration. Scale bar indicates 100 μm (magnification 20X).

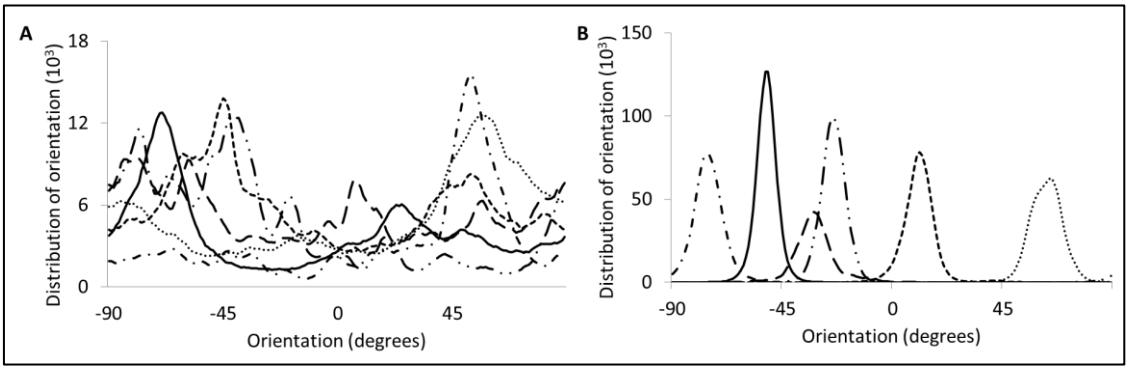

Figure 3-4: Quantification of fiber alignment for a) unaligned and b) aligned PCL and PCL/PLGA scaffolds. Solid lines represent 15% w/v PCL, dotted lines represent 15%w/v PCL with 25% PLGA, dashed lines represent 15%w/v PCL with 50% PLGA, dot-dashed lines represent 20% w/v PCL, dot-dot-dashed lines represent 20%w/v PCL with 25% PLGA, and lighter dotted lines represent 20%w/v PCL with 50% PLGA.

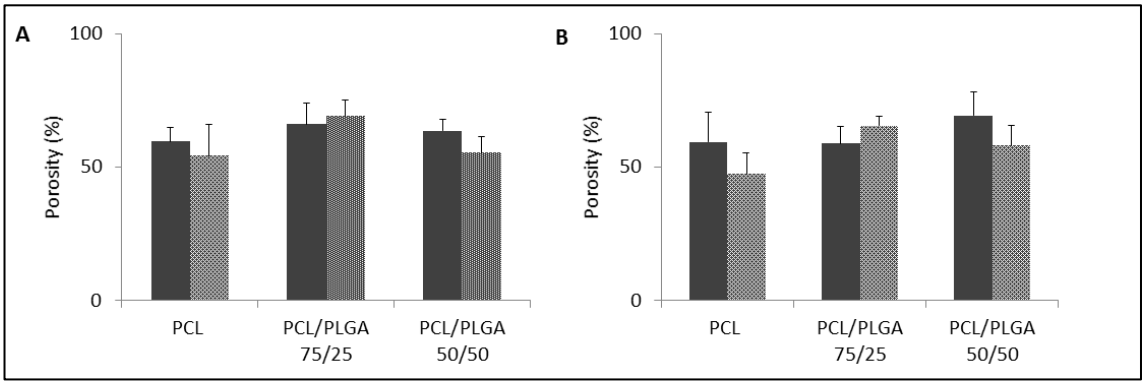

Figure 3-5: Quantification of the porosity of the A) unaligned and B) aligned electrospun scaffolds of PCL and PCL/PLGA (75/25 and 50/50). Solid bars represent 15% w/v fibers and dotted bars represent 20% w/v fibers. Bars indicate standard deviation

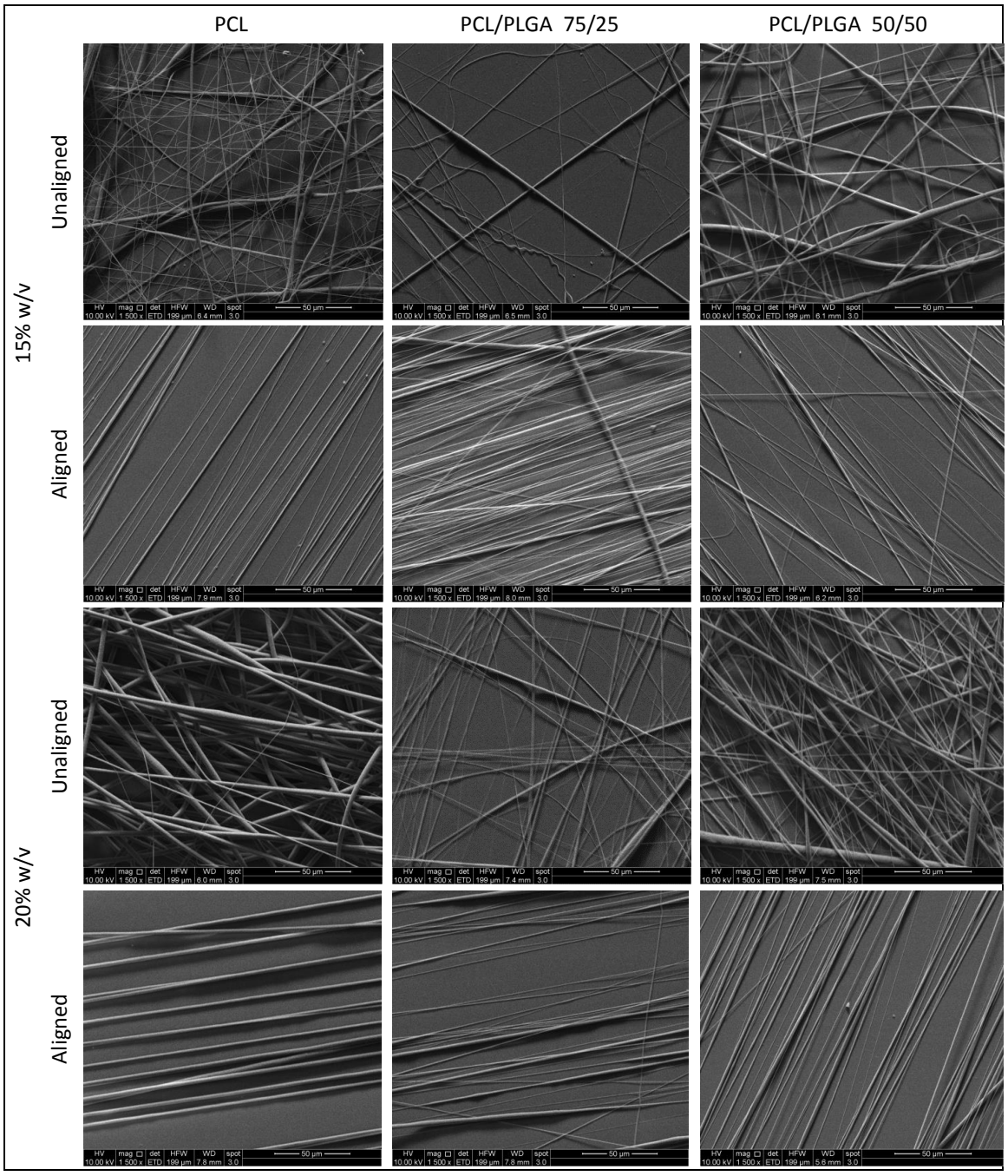

Figure 3-6: Scanning electron microscopy micrographs of aligned and unaligned electrospun scaffolds of PCL and PCL/PLGA blends prepared in 15% and 20% w/v concentrations at 1500X magnification.

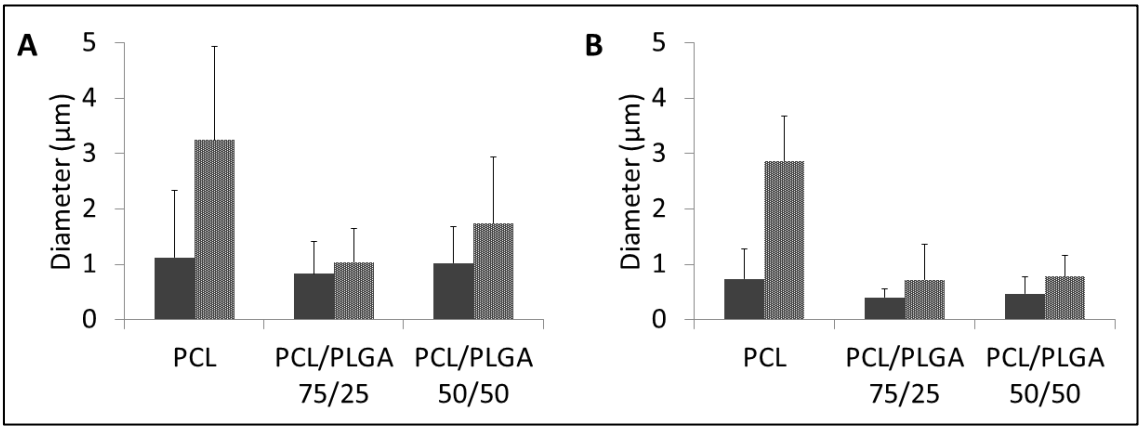

Figure 3-7: Quantification of the diameter of A) unaligned and B) aligned electrospun scaffolds of PCL and PCL/PLGA (75/25 and 50/50). Solid bars represent 15% w/v fibers and dotted bars represent 20% w/v fibers. Bars indicate standard deviation.

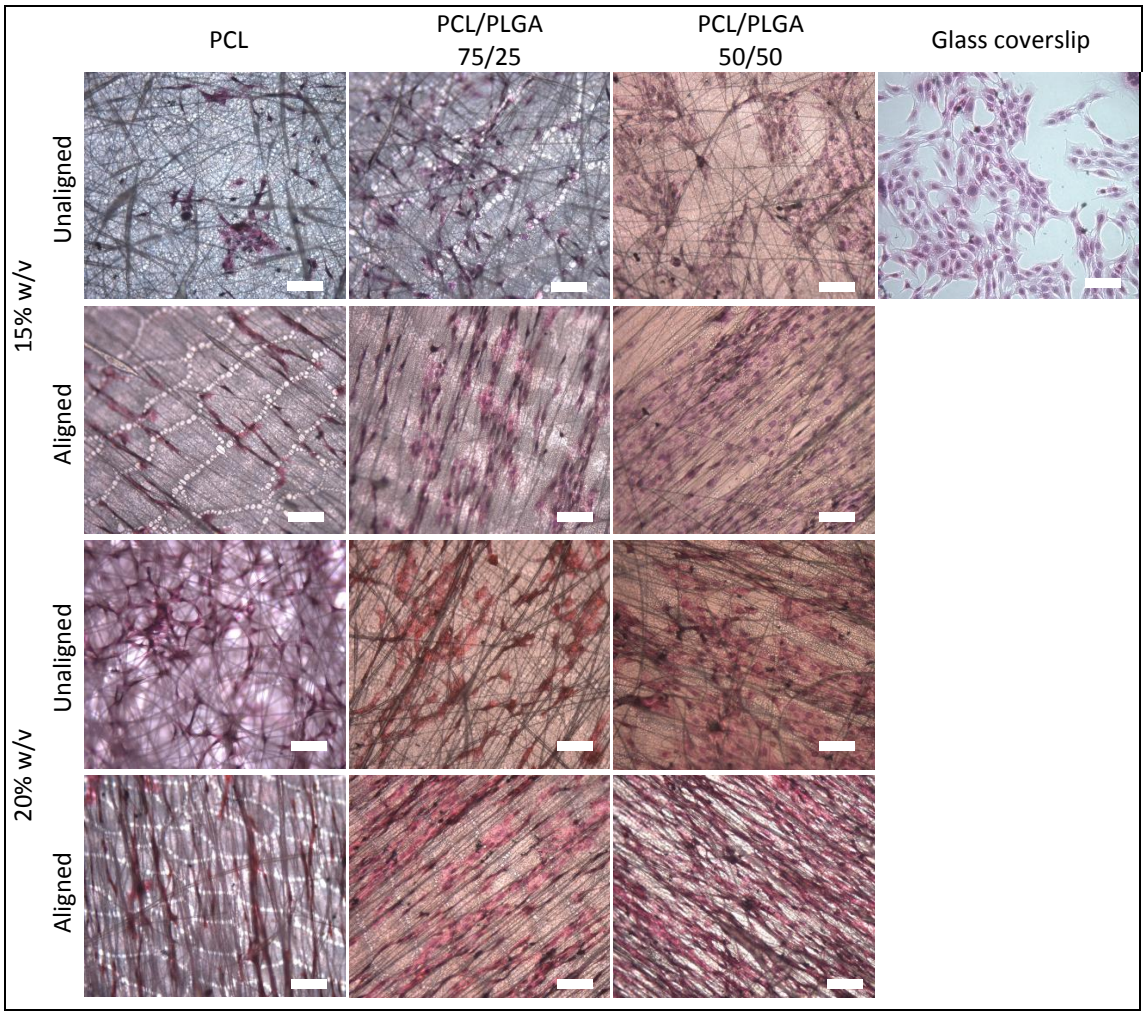

Figure 3-8: Transmitted light microscopy micrographs of electrospun scaffolds with C2C12 cells stained with haematoxylin (nucleus) and eosin (cytoplasm). Cells were fixed and marked after 5 days. Scale bar indicates 100 μm (magnification 20X).

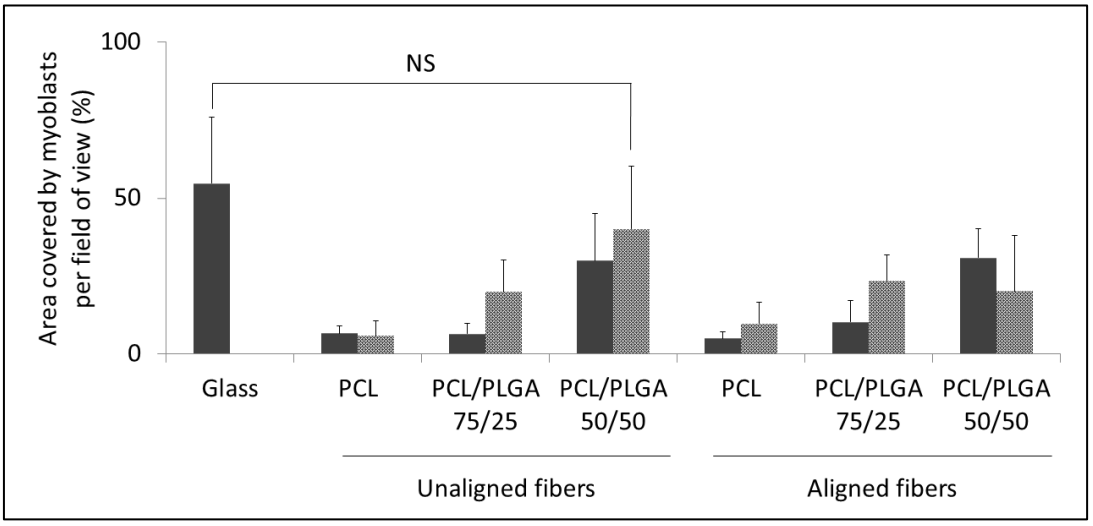

Figure 3-9: Quantification of area covered by myoblasts per field of view (at magnification 20X) on electrospun PCL and PCL/PLGA scaffolds after 5 days of incubation. Solid bars represent 15% w/v fibers and dotted bars represent 20% w/v fibers. Bars indicate standard deviation. NS indicates no statistical difference (p-value ≥ 0.05).

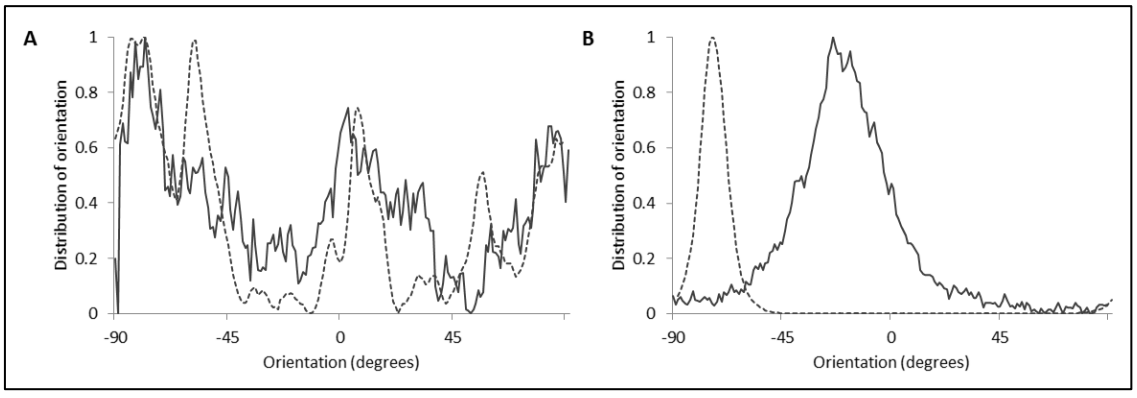

Figure 3-10: Quantification of nuclei and fiber alignment for myoblasts on A) unaligned and B) aligned 20% w/v PCL scaffolds. Solid lines represent nuclei on 20% w/v PCL fibers, and dashed lines represent 20% w/v PCL fibers. All curves were normalized.

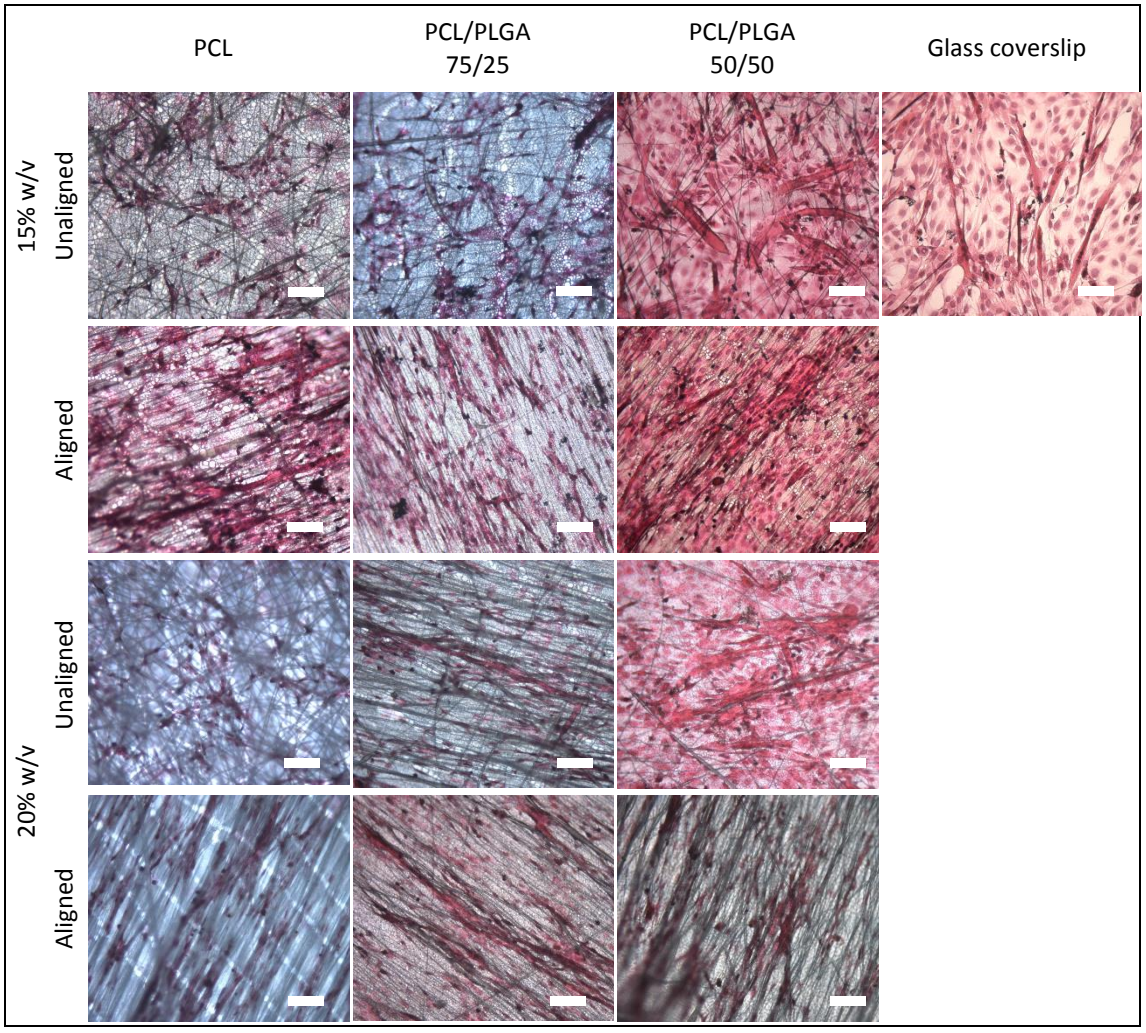

Figure 3-11: Transmitted light microscopy micrographs of electrospun scaffolds with C2C12 cells stained with haematoxylin (nucleus) and eosin (cytoplasm). Cells were fixed and marked after 7 days. Scale bar indicates 100 μm (magnification 20X).

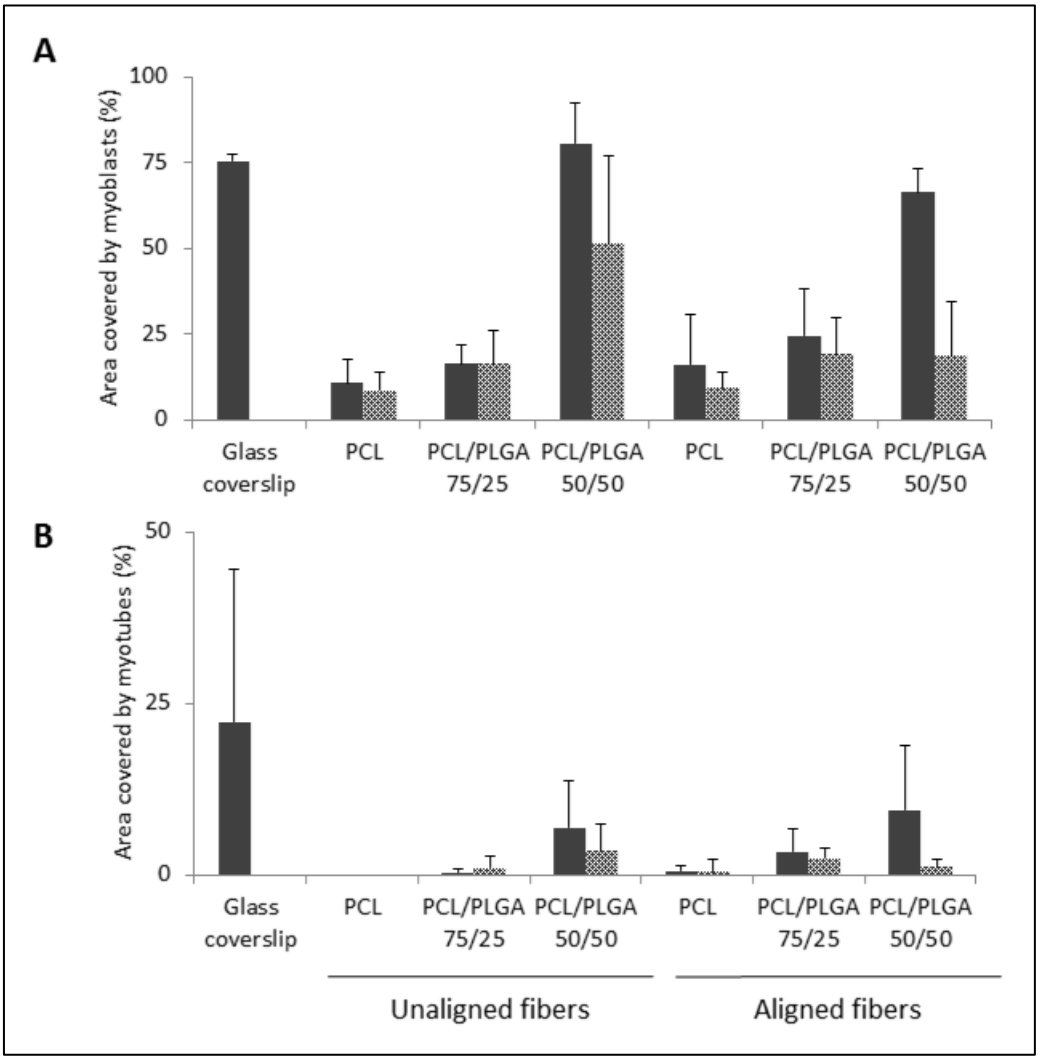

Figure 3-12: Quantification of area covered by a) myoblasts and b) myotubes per field of view (at magnification 20X) on electrospun PCL and PCL/PLGA scaffolds after 7 days of incubation. Solid bars represent 15% w/v fibers and dotted bars represent 20% w/v fibers. Bars indicate standard deviation.

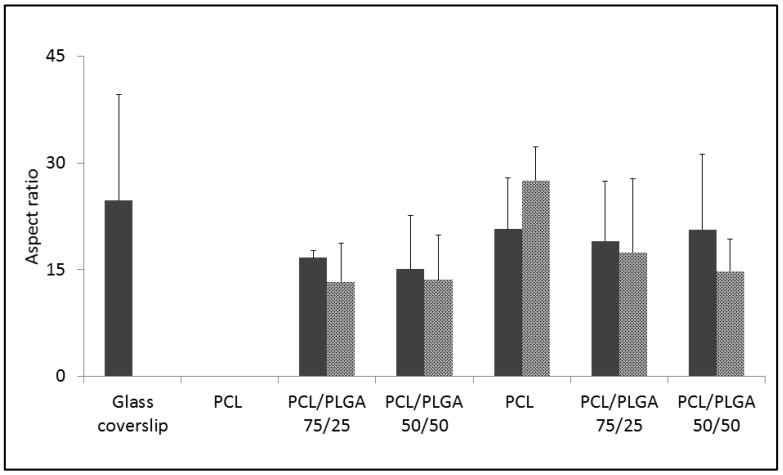

Figure 3-13: Quantification of elongation of myotubes on electrospun PCL and PCL/PLGA fibers. Solid bars represent 15% w/v fibers and dotted bars represent 20% w/v fibers. Bars indicate standard deviation.

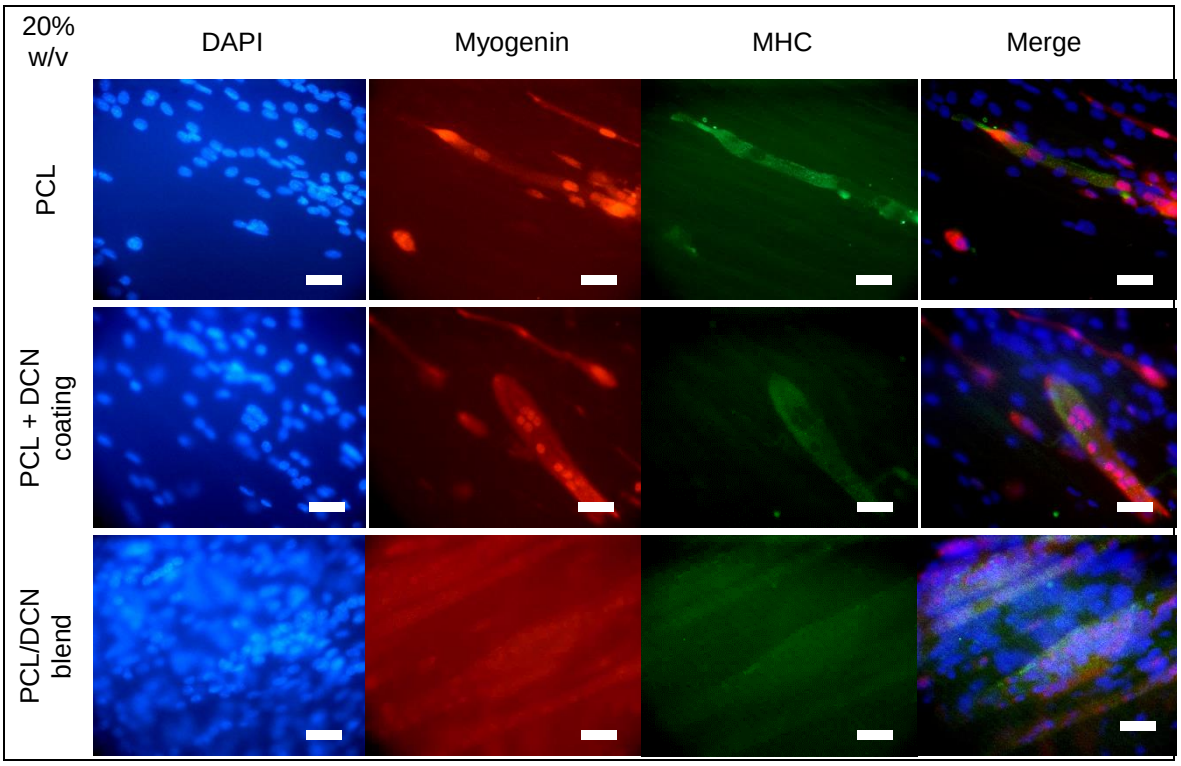

Figure 3-14: Fluorescent microscope images of C2C12 cells marked for myogenin (red), MHC (green) and nucleus (blue) on 20% w/v PCL aligned fibers with and without decorin. Cells were fixed and marked after 12 days. Scale bar indicates 50 μm (magnification 40X).

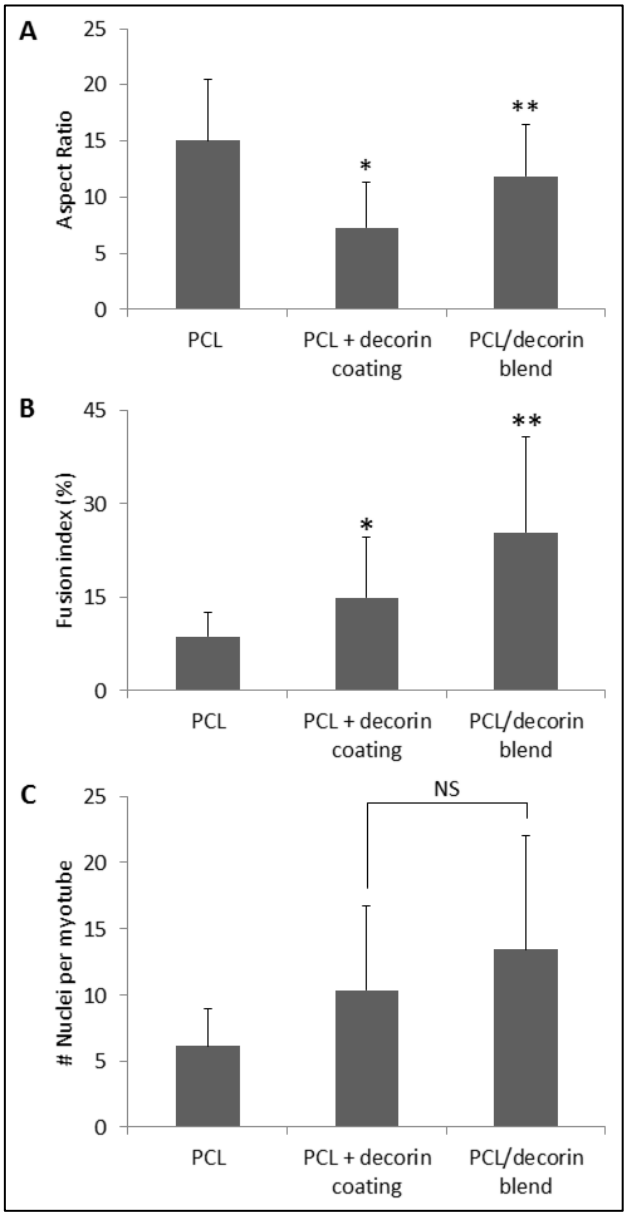

Figure 3-15: Quantification of a) elongation of myotubes on electrospun PCL fibers with or without decorin, b) nuclei per myotube on electrospun PCL fibers with or without decorin, c) nuclei and fiber orientation on 20% w/v PCL scaffolds with and without decorin. Bars indicate standard deviation. Stars indicate statistical difference (p-value < 0.05). NS indicates no statistical difference (p-value ≥ 0.05).

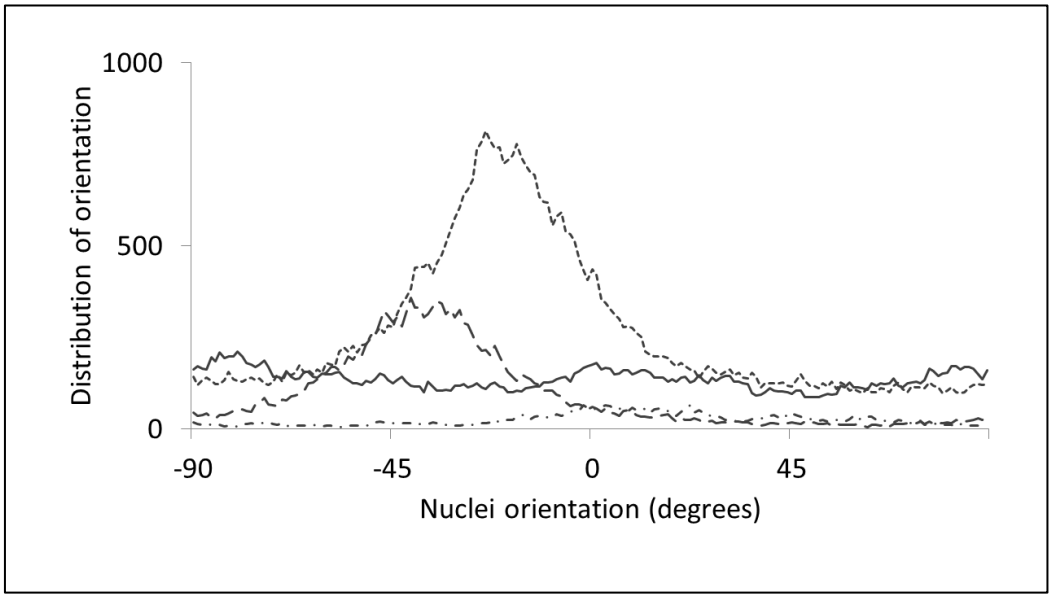

Figure 3-16: Quantification of nuclei and fiber orientation on 20% w/v PCL scaffolds with and without decorin. The solid line represents 20% w/v PCL unaligned fibers, the dotted line represents 20% w/v PCL aligned fibers, the dashed line represents 20% w/v PCL aligned fibers + decorin coating, and the dashed-dotted line represents 20% w/v PCL/decorin aligned fibers.

3.9 Tables

Table 3-1: Melting and glass transition temperatures of PCL and PCL/PLGA blends obtained from DSC thermograms. (* values were obtained from Sigma-Aldrich).

	PCL	PCL/PLGA 75/25	PCL/PLGA 50/50	PLGA
T_g	-61.36°C	-62.16°C	-60.8°C	49-55°C
T_m	57.56°C	55.39°C	55.39°C	225-230°C

Table 3-2: Kurtosis values for fiber alignment of unaligned and aligned 15% w/v and 20% w/v PCL and PCL/PLGA scaffolds.

Alignment	Concentration	PCL	PCL/PLGA 75/25	PCL/PLGA 50/50
Unaligned	15%	2.57	1.00	-0.61
	20%	4.87	-0.77	0.10
Aligned	15%	14.85	10.12	8.00
	20%	8.85	10.77	6.60

Table 3-4: Kurtosis values for fiber and myoblast nuclei orientation curves on unaligned and aligned 20% w/v PCL scaffolds.

	PCL unaligned	PCL aligned	nuclei on PCL unaligned	nuclei on PCL aligned
Kurtosis	4.87	8.85	-0.16	0.49

4. FURTHER DISCUSSION

In addition to the results and discussion included in this thesis, other experiments were carried out, which improved the fabrication of the fibers and mechanically characterized the fibers.

Humidity is an important factor in the electrospinning process. During the winter months, on rainy days the relative humidity reached well over 50%. In these environmental conditions, it was very difficult, if not impossible, to electrospin fibers. When fibers were produced, these were full of beads. Therefore, it is important to make sure that the humidity is under 45%, ideally around 30%. This can be attained by electrospinning in dry climates (summer and spring seasons in Santiago, Chile) or under humidity control conditions. This last option is ideal, but since we did not have access to such equipment, we used an extraction hood to bring down the humidity inside the hood and avoid electrospinning in rainy days. It is also important to only use the extraction fan previous to electrospinning. The airflow affects the jet stream causing loss of electrospun material and alignment.

Solvent is another important factor in the electrospinning process. In the beginning, we used tetrahydrofuran (THF) to prepare the polymer solutions. Electrospinning PCL in THF produced beadless fibers, but it required a much higher applied voltage (> 20 kV), which produced a lot of electrical discharge. Electrospinning PCL/PLGA blends in THF was very difficult and the produced fibers had many beads. We later changed the solvent for chloroform, which improved the quality (i.e., beadless and more uniform) and the reproducibility of the fibers on both PCL and PCL/PLGA blends, and the applied voltage required to electrospun these fibers lowered to 12kV. Since THF has a high electrical conductivity (4.5×10^{-5} S/cm), the Taylor cone produced with was not stable, which in turn caused spattering and bead formation. Chloroform on the other hand, has low electrical conductivity ($<1 \times 10^{-10}$ S/cm) producing a stable Taylor cone and beadless fibers. Therefore, we used chloroform for the polymer solutions for the experimental setting.

It is important to electrospin all polymer solutions for the same amount of time or total volume, considering that flow rate is maintained. It is also very important to constantly clean the needle-tip for any accumulation of solution. This will minimize loss of solution and will help control fiber density (measured as substrate porosity).

The tensile strength of the fibers was measured using the three-point flexural test via Atomic Force Micrscopy (AFM) (see Annex A). At first, we had tried to create channels of < 20 μm in width with glass coverslips. This method consisted in using a glass cutter to break a coverslip in half and then adhering these two pieces onto another coverslip in such a way that the pieces would be separated by a < 20μm fissure. We would later find that the two cut pieces were not level with each other and this would cause the cantilever tip to break as it tried to scan the fiber previous to the flexural test. The method we decided to use consisted in using the overlapping (topmost) fiber of two intersecting fibers. However, we were unable to measure the length of suspended fiber and therefore were unable to obtain a Young's modulus. For this reason, a "relative elastic modulus" was measured. It is worth noting that three-point flexural test measures tensile strength of the individual fibers. Alignment is not a factor. A more accurate measurement of tensile strength for the fiber substrate would be to measure tensile strength of the entire scaffold with a texturometer. From the three-point flexural test, we found that PLGA had a higher "relative" elastic modulus than PCL. This means that PLGA is a stiffer and less elastic polymer than PCL. By adding PLGA to PCL, we can increase scaffold stiffness. Fibers with 50% PLGA have the greatest stiffness. Substrate stiffness is important for myoblast proliferation and differentiation (see Chapter 3).

With this study, we can improve scaffolds for applications in skeletal muscle regeneration by promoting proliferation and differentiation. We are able to control cell alignment by fiber orientation. We are able to increase myoblast proliferation with the addition of PLGA. Differentiation increases significantly with the addition of decorin and myotubes are also longer and thicker with the addition of this protein. Therefore, these types of scaffolds can be used for in vitro growth and maturation of myoblasts into aligned myotubes for later implantation in organisms. Future work includes the fabrication of 3D

scaffolds and the incorporation of conductive polymers such as poly(octanoic acid 2-thiophen-3-yl-ethyl ester) (poly(OTE)). Knowing that skeletal muscles are stimulated with electrical impulses to contract, the addition of conductive polymers proves to be beneficial for myoblast proliferation and for maintaining regeneration potential. Considering this, work is currently being done to be able to measure the conductivity of myoblasts and scaffolds, so that we may be able to later control the conductive properties of scaffolds to best simulate the microenvironment of skeletal muscle tissue.

BIBLIOGRAPHY

Abdellatef, S. A., Ohi, A., Nabatame, T., & Taniguchi, A. (2014). The effect of physical and chemical cues on hepatocellular function and morphology. *International Journal of Molecular Sciences*, *15*(3), 4299–4317.

Amthor, H., Nicholas, G., McKinnell, I., Kemp, C. F., Sharma, M., Kambadur, R., & Patel, K. (2004). Follistatin complexes Myostatin and antagonises Myostatin-mediated inhibition of myogenesis. *Developmental Biology*, *270*(1), 19–30.

Andres, V., & Walsh, K. (1996). Myogenin expression, cell cycle withdrawl, and phenotypic differentiation are temproarily seperable events that precede cell fusion upon myogenesis. *Journal of Cell Biology*, *132*(4), 657–666.

Andres-Mateos, E., Mejias, R., Soleimani, A., Lin, B. M., Burks, T. N., Marx, R., … Cohn, R. D. (2012). Impaired Skeletal Muscle Regeneration in the Absence of Fibrosis during Hibernation in 13-Lined Ground Squirrels. *PLoS ONE*, *7*(11), 1–10.

Baumgart, F., & Cordey, J. (2001). Stiffness - An unknown world of mechanical science? *Injury*, *32*.(SUPPL. 2), 1-14.

Boonen, K. J. M., Rosaria-Chak, K. Y., Baaijens, F. P. T., van der Schaft, D. W. J., & Post, M. J. (2009). Essential environmental cues from the satellite cell niche: optimizing proliferation and differentiation. *American Journal of Physiology. Cell Physiology*, *296*, C1338–C1345.

Brandan E, Fuentes ME, Andrade W. (1991). The proteoglycan decorin is synthesized and secreted by differentiated myotubes. *Eur J Cell Biol*. 55, 209–16.

Burkitt, H. G., Barbara, Y., & Heath, John, W. (1995). *Wheater's Functional Histology*. New York: Churchill Livingstone.

Cappella, B., & Dietler, G. (1999). Force-distance curves by atomic force microscopy. *Surface Science Reports*, *34*(1–3), 1–104.

Chen, E. H., Grote, E., Mohler, W., & Vignery, A. (2007). Cell-cell fusion. *FEBS Letters*, *581*(11), 2181–2193.

Chen, J. L., Colgan, T. D., Walton, K. L., Gregorevic, P., & Harrison, C. A. (2016). The TGF-β Signalling Network in Muscle Development, Adaptation and Disease. In J. White & G. Smythe (Eds.), (Vol. 900, pp. 97–131). Cham: Springer International Publishing.

Choi, J. S., Lee, S. J., Christ, G. J., Atala, A., & Yoo, J. J. (2008). The influence of

electrospun aligned poly(epsilon-caprolactone)/collagen nanofiber meshes on the formation of self-aligned skeletal muscle myotubes. *Biomaterials*, *29*(19), 2899–906.

Ciardelli, G., Chiono, V., Vozzi, G., Pracella, M., Ahluwalia, A., Barbani, N., … Giusti, P. (2005). Blends of poly-(epsilon-caprolactone) and polysaccharides in tissue engineering applications. *Biomacromolecules*, *6*(4), 1961–1976.

Croisier, F., Duwez, a. S., Jérôme, C., Léonard, a. F., Van Der Werf, K. O., Dijkstra, P. J., & Bennink, M. L. (2012). Mechanical testing of electrospun PCL fibers. *Acta Biomaterialia*, *8*(1), 218–224.

Deitzel, J. ., Kleinmeyer, J., Harris, D., & Beck Tan, N. . (2001). The effect of processing variables on the morphology of electrospun nanofibers and textiles. *Polymer*, *42*(1), 261–272.

Elzein, T., Nasser-Eddine, M., Delaite, C., Bistac, S., & Dumas, P. (2004). FTIR study of polycaprolactone chain organization at interfaces. *Journal of Colloid and Interface Science*, *273*(2), 381–387.

Engler, A. J., Griffin, M. A., Sen, S., B??nnemann, C. G., Sweeney, H. L., & Discher, D. E. (2004). Myotubes differentiate optimally on substrates with tissue-like stiffness: Pathological implications for soft or stiff microenvironments. *Journal of Cell Biology*, *166*(6), 877–887.

Engler, A. J., Sen, S., Sweeney, H. L., & Discher, D. E. (2006). Matrix Elasticity Directs Stem Cell Lineage Specification. *Cell*, *126*(4), 677–689.

Fisher, J. P. (2007). *Tissue Engineering*. Springer Science & Business Media.

Fung, Y. C. (1993). *Biomechanics: Mechanical Properties of Living Tissues* (2nd Editio). New York: Springer-Verlag.

Garg, K., & Bowlin, G. L. (2011). Electrospinning jets and nanofibrous structures. *Biomicrofluidics*, *5*(1), 1–19.

Gentile, P., Chiono, V., Carmagnola, I., & Hatton, P. V. (2014). An overview of poly(lactic-co-glycolic) Acid (PLGA)-based biomaterials for bone tissue engineering. *International Journal of Molecular Sciences*, *15*(3), 3640–3659.

Giri, S. N., Hyde, D. M., Braun, R. K., Gaarde, W., Harper, J. R., & Pierschbacher, M. D. (1997). Antifibrotic effect of decorin in a bleomycin hamster model of lung fibrosis. *Biochemical Pharmacology*, *54*(11), 1205–1216.

Grasman, J. M., Zayas, M. J., Page, R., & Pins, G. D. (2015). Biomimetic Scaffolds for

Regeneration of Volumetric Muscle Loss in Skeletal Muscle Injuries. *Acta Biomaterialia*, *25*, 2–15.

Haider, S., Al-Zeghayer, Y., Ahmed Ali, F. A., Haider, A., Mahmood, A., Al-Masry, W. A., … Aijaz, M. O. (2013). Highly aligned narrow diameter chitosan electrospun nanofibers. *Journal of Polymer Research*, *20*(4).

Hiep, N. T., & Lee, B. T. (2010). Electro-spinning of PLGA/PCL blends for tissue engineering and their biocompatibility. *Journal of Materials Science: Materials in Medicine*, *21*, 1969–1978.

Hinderer, S., Schesny, M., Bayrak, A., Ibold, B., Hampel, M., Walles, T., … Schenke-Layland, K. (2012). Engineering of fibrillar decorin matrices for a tissue-engineered trachea. *Biomaterials*, *33*(21), 5259–5266.

Hocking, A. M., Shinomura, T., & McQuillan, D. J. (1998). Leucine-rich repeat glycoproteins of the extracellular matrix. *Matrix Biology*, *17*(1), 1–19.

Hotaling, N. A., Bharti, K., Kriel, H., & Simon, C. G. (2015). DiameterJ: A validated open source nanofiber diameter measurement tool. *Biomaterials*, *61*, 327–338.

Huang, N. F., Patel, S., Thakar, R. G., Wu, J., Hsiao, B. S., Chu, B., … Li, S. (2006). Myotube assembly on nanofibrous and micropatterned polymers. *Nano Letters*, *6*(3), 537–542.

Junqueira, L. C., & Carneiro, J. (1995). *Basic Histology*. Stamford: Appleton and Lange.

Karalaki, M., Fili, S., Philippou, A., & Koutsilieris, M. (2009). Muscle regeneration: cellular and molecular events. *In Vivo (Athens, Greece)*, *23*(5), 779–96.

Kemala, T., Budianto, E., & Soegiyono, B. (2012). Preparation and characterization of microspheres based on blend of poly(lactic acid) and poly(??-caprolactone) with poly(vinyl alcohol) as emulsifier. *Arabian Journal of Chemistry*, *5*(1), 103–108.

Kim, J. Y., & Cho, D. W. (2009). Blended PCL/PLGA scaffold fabrication using multi-head deposition system. *Microelectronic Engineering*, *86*(4–6), 1447–1450.

Langer, R., & Tirrell, D. a. (2004). Designing materials for biology and medicine. *Nature*, *428*(6982), 487–492.

Langhammer, C. G., Kutzing, M. K., Luo, V., Zahn, J. D., & Firestein, B. L. (2013). A topographically modified substrate-embedded MEA for directed myotube formation at electrode contact sites. *Annals of Biomedical Engineering*, *41*(2), 408–420.

Leach, M. K., Feng, Z.-Q., Gertz, C. C., Tuck, S. J., Regan, T. M., Naim, Y., … Corey, J. M. (2011). The culture of primary motor and sensory neurons in defined media on electrospun poly-L-lactide nanofiber scaffolds. *Journal of Visualized Experiments : JoVE*, (48), 1–5.

Li, W.-J., & Tuan, R. S. (2009). Fabrication and application of nanofibrous scaffolds in tissue engineering. *Current Protocols in Cell Biology / Editorial Board, Juan S. Bonifacino ... [et Al.]*, *Chapter 25*, Unit 25.2.

Li, X., McFarland, D. C., & Velleman, S. G. (2006). Effect of transforming growth factor-beta on decorin and beta1 integrin expression during muscle development in chickens. *Poultry Science*, *85*(2), 326–32.

Li, Y., Cummins, J., & Huard, J. (2001). Muscle injury and repair. *Current Opinion in Orthopaedics*, *12*, 409–415.

Li, Y., Huang, Z., & Lü, Y. (2006). Electrospinning of nylon-6,66,1010 terpolymer. *European Polymer Journal*, *42*(7), 1696–1704.

Li, Y., Li, J., Zhu, J., Sun, B., Branca, M., Tang, Y., … Huard, J. (2007). Decorin Gene Transfer Promotes Muscle Cell Differentiation and Muscle Regeneration. *Molecular Therapy*, *15*(9), 1616–1622.

Lieber, R. (2002). Skeletal muscle structure, function, and plasticity. Lippincott Williams and Wilkins, 2nd ed., p. 18.

Markaki, A. E., & Clyne, T. W. (2003). Mechanics of thin ultra-light stainless steel sandwich sheet material: Part I. Stiffness. *Acta Materialia*, *51*(5), 1341–1350.

Matabola, K. P., & Moutloali, R. M. (2013). The influence of electrospinning parameters on the morphology and diameter of poly(vinyledene fluoride) nanofibers-Effect of sodium chloride. *Journal of Materials Science*, *48*(16), 5475–5482.

Megelski, S., Stephens, J. S., Bruce Chase, D., & Rabolt, J. F. (2002). Micro- and nanostructured surface morphology on electrospun polymer fibers. *Macromolecules*, *35*(22), 8456–8466.

Meng, X., Leslie, P., Zhang, Y., & Dong, J. (2014). Stem cells in a three-dimensional scaffold environment. *SpringerPlus*, *3*(1), 80.

Mescher, A. L. (2016). *Junqueira ' s Basic Histology Text & Atlas (14th ed .)* (14th ed.). McGraw-Hill.

Nair, L. S., & Laurencin, C. T. (2007). Biodegradable polymers as biomaterials.

Progress in Polymer Science (Oxford), *32*(8–9), 762–798.

Nishimura, T., Futami, E., Taneichi, A., Mori, T., & Hattori, A. (2002). Decorin expression during development of bovine skeletal muscle and its role in morphogenesis of the intramuscular connective tissue. *Cells Tissues Organs*, *171*(2–3), 199–214.

Noble, N. A., Harper, J. R., & Border, W. A. (1993). In Vivo Interactions of TGF-β and Extracellular Matrix, *Progress in Growth Factor Research*, *4*, 369–382.

Nourmohammadi, J., Ghaee, A., & Liavali, S. H. (2016). Preparation and characterization of bioactive composite scaffolds from polycaprolactone nanofibers-chitosan-oxidized starch for bone regeneration. *Carbohydrate Polymers*, *138*, 172–179.

Olguin, H. C., & Olwin, B. B. (2004). Pax-7 up-regulation inhibits myogenesis and cell cycle progression in satellite cells: A potential mechanism for self-renewal. *Developmental Biology*, *275*(2), 375–388.

Olguin, H., & Enrique, B. (2002). Decorin is required to maintain commited skeletal muscle cell population grouped allowing normal differentiation in vivo. In *MOLECULAR BIOLOGY OF THE CELL* (Vol. 13, p. 341A). AMER SOC CELL BIOLOGY.

Padilla, C., Ramos, A., González, N., Isaacs, M., Zacconi, F., Olguín, H. C., & Valenzuela, L. M. (2016). Chitosan/poly-octanoic acid 2-thiophen-3-yl-ethyl ester blends as a scaffold to maintain myoblasts regeneration potential in vitro. *Journal of Biomedical Materials Research. Part A*.

Piskin, E. (1994). Journal of Biomaterials Science , Biodegradable polymers as biomaterials, (March 2013), 37–41.

Ratner, B. D. (2004). *Biomaterials Science: An Interdisciplinary Endeavor*. *Biomaterials Science - An Introduction to Materials in Medicine*.

Ren, K., Crouzier, T., Roy, C., & Picart, C. (2008). Polyelectrolyte multilayer films of controlled stiffness modulate myoblast cell differentiation. *Advanced Functional Materials*, *18*(9), 1378–1389.

Rodriguez, F., Cohen, C., Ober, C. K., & Archer, L. A. (2014). *Principles of Polymer Systems* (6th Edition). CRC Press.

Romanazzo, S., Forte, G., Ebara, M., Uto, K., Pagliari, S., Aoyagi, T., … Taniguchi, A. (2012). Substrate stiffness affects skeletal myoblast differentiation in vitro. *Science and Technology of Advanced Materials*, *13*(6), 64211.

Sartori, R., Gregorevic, P., & Sandri, M. (2014). TGF?? and BMP signaling in skeletal muscle: Potential significance for muscle-related disease. *Trends in Endocrinology and Metabolism*, *25*(9), 464–471.

Schneider, C. a, Rasband, W. S., & Eliceiri, K. W. (2012). NIH Image to ImageJ: 25 years of image analysis. *Nature Methods*, *9*(7), 671–675.

Ständer, M., Naumann, U., Dumitrescu, L., Heneka, M., Löschmann, P., Gulbins, E., … Weller, M. (1998). Decorin gene transfer-mediated suppression of TGF-beta synthesis abrogates experimental malignant glioma growth in vivo. *Gene Therapy*, *5*(9), 1187–1194.

Tan, E. P. S., Ng, S. Y., & Lim, C. T. (2005). Tensile testing of a single ultrafine polymeric fiber. *Biomaterials*, *26*(13), 1453–1456.

Tang, Z. G., Callaghan, J. T., & Hunt, J. A. (2005). The physical properties and response of osteoblasts to solution cast films of PLGA doped polycaprolactone. *Biomaterials*, *26*(33), 6618–6624.

Trensz, F., Lucien, F., Couture, V., Söllrald, T., Drouin, G., Rouleau, A.-J., … Grenier, G. (2015). Increased microenvironment stiffness in damaged myofibers promotes myogenic progenitor cell proliferation. *Skeletal Muscle*, *5*, 5.

Webster, M. T., Manor, U., Lippincott-Schwartz, J., & Fan, C. M. (2016). Intravital Imaging Reveals Ghost Fibers as Architectural Units Guiding Myogenic Progenitors during Regeneration. *Cell Stem Cell*, *18*(2), 243–252.

Westfall, P. H. (2015). Kurtosis as Peakedness, 1905 - 2014. R.I.P. *The American Statistician*, *68*(3), 191–195.

Whited, B. M., & Rylander, M. N. (2014). The influence of electrospun scaffold topography on endothelial cell morphology, alignment, and adhesion in response to fluid flow. *Biotechnology and Bioengineering*, *111*(1), 184–195.

Yannas, I. V. (2004). “Classes of materials used in medicine: natural materials,” in Biomaterials Science—An Introduction to Materials in Medicine, B. D. Ratner, A. S. Hoffman, F. J. Schoen, and J. Lemons, Eds., Elsevier Academic Press, San Diego, Calif, USA, 127–136.

A N N E X E S

ANNEX A: TENSILE STRENGTH ANALYSIS OF POLYMER FIBERS VIA ATOMIC FORCE MICROSCOPY

Topography and tensile strength were analyzed with atomic force microscopy (AFM) using the AFM microscope Innova (Bruker). Images were obtained in the tapping mode using a silicon tip cantilever without coating (Asylum Research model AC240TS-R3). Data was collected with Nanodrive software (Bruker).

Polymer fibers were electrospun directly onto glass coverslips for 5 minutes to obtain aligned fibers. Presence and morphology of the fibers was confirmed by optical microscopy (Olympus model CKX41SF). Topography and tensile strength were analyzed with the Innova Atomic Force Microscope (Bruker). Images were obtained in the tapping mode using a silicon tip cantilever without coating (Asylum Research model AC240TS-R3).

To measure tensile strength, overlapping fibers were selected using transmitted light microscopy. According to Croisier et al. (2012), polymeric fibers directly on glass and glass substrates have no significant difference in dF/dz values. Therefore, it is valid to use an underlying fiber as a supporting pin to carry out the three-point flexural test. Intersecting fibers were selected and their topography was analyzed by using the tapping method. By analyzing height topography, the overlaying fiber was determined and then at least 20 points were selected on the suspended portion of this fiber as shown in Figure A-1. Using SPMLab software, deflection vs. displacement curves were obtained for each of the selected points on the suspended fiber. In the bending tests, the cantilever was displaced over a range of 0.5 – 1 μm.

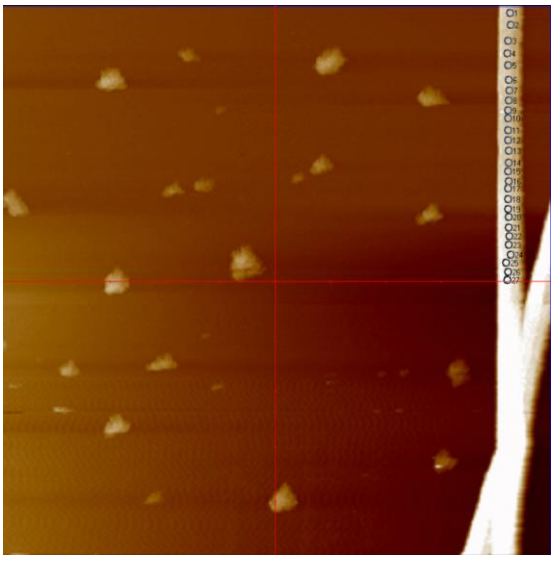

Figure A-1: Probe positions (circles) set on overlapping 15%w/v PCL fiber for single point spectroscopy **(SPS).** After fibers were scanned in tapping mode with AFM, the overlapping fiber was determined and 20+ probe positions were set on that fiber (small circles on the image) to measure dF/dz in an area of 20x20μm^2.

For each deflection vs. displacement curve, only the withdrawal curves were considered (Figure A-2). Approach curves were disregarded because of the deformation that occurs on the polymer when the cantilever presses into the fiber. Given the elasto-plastic nature of the materials, the withdraw curves contain a reduced effect of the deformation of the fiber (Cappella & Dietler, 1999).
Deflection vs. displacement curves obtained as shown in Figure A-2. If we consider Hooke's Law,

$$F = k\,z \tag{A.1}$$

the slope (dF/dz) of the curves is comparable to the spring constant k. The slope of the curves was determined by a fitting a linear curve on the contact region, that is to say, the linear portion until the jump-off-contact point (Safanama et al.,2012).

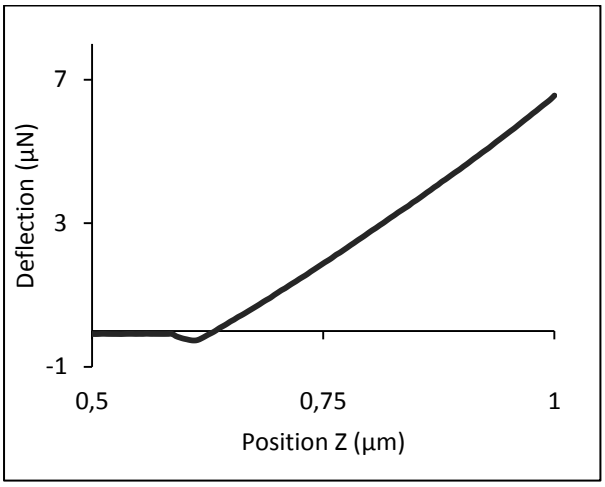

Figure A-2: Representation of F/z curves (withdraw) obtained with AFM at one position along a suspended fiber. This is the trace or withdrawal curve of a PCL/PLGA 75/25 fiber.

Croiser et al. states that the bending modulus (E) can be obtained with the following equations:

$$E = \frac{L^3}{48I}\frac{dF}{dz} \tag{A.2}$$

$$I = \frac{\pi}{4}R^4 \tag{A.3}$$

in which L is the length of the suspended portion of electrospun fiber, R is the radius of the fiber, and dF/dz is the slope of the force-distance curves. Croiser et al. also states that the bending modulus is similar to the Young's modulus for rods with high length-to-diameter ratios. Therefore, bending modulus can be considered equivalent to the Young's modulus for these electrospun fibers. The radius for the measured fibers was determined by AFM prior to SPS.

Results

Topography images of fiber scaffolds show that the fibers are not perfectly smooth (Figure A-1). These images also confirm the value and variability of fiber diameters obtained via SEM (in Chapter 3 of this thesis).

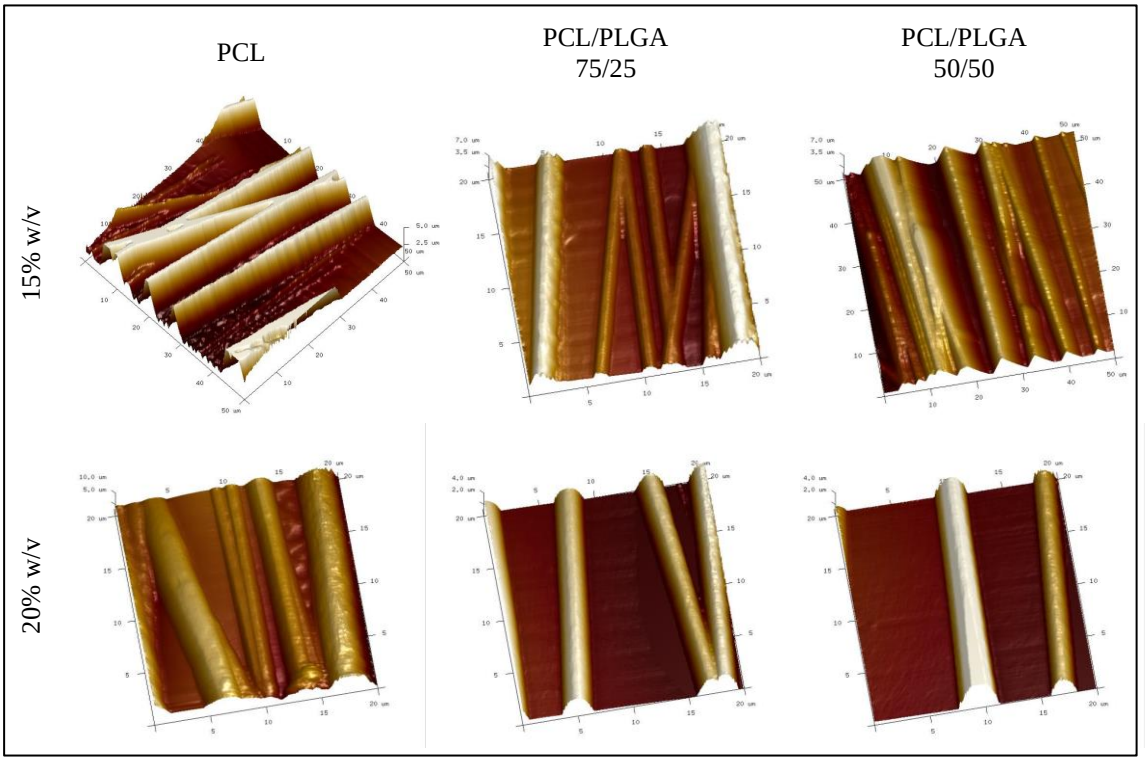

Figure A-3: Topography diagrams of obtained from AFM of aligned fibers of different compositions (PCL and PCL/PLGA blends) and different diameters (produced by different polymer concentrations of 15 and 20% w/v). Fiber scaffolds were scanned over a 20 μm x 20 μm area.

A summary of dF/dz of the different fiber types (blends of 75/25 and 50/50 PCL/PLGA) is shown in Figure A-4. Average dF/dz for PCL, PCL/PLGA (75/25 and 50/50) are 24.09 μN/μm, 17.28 μN/μm, and 18.91 μN/μm respectively.

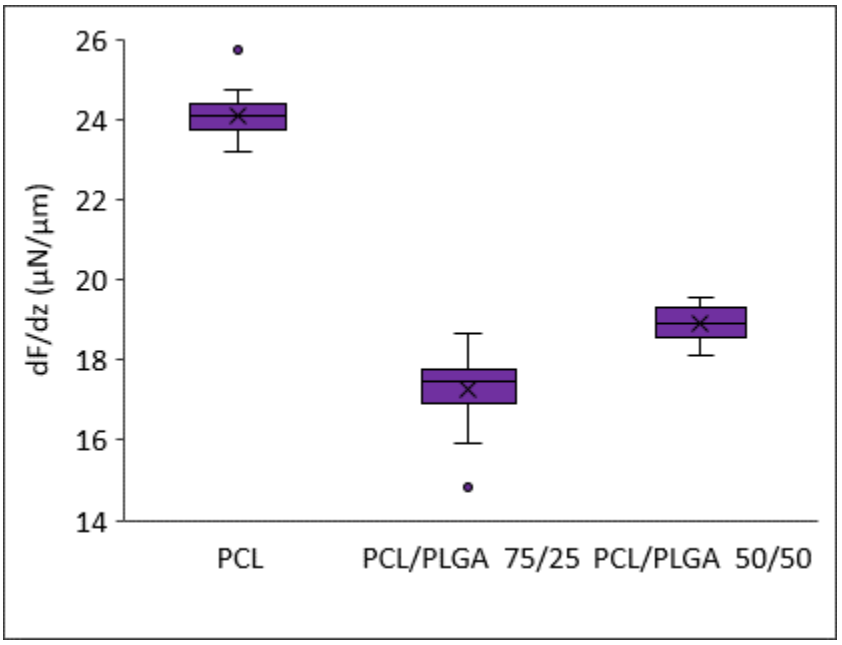

Figure A-4: Boxplot of dF/dz values of fibers of PCL and PCL/PLGA blends (75/25 and 50/50). Vertical axis is truncated and begins at 14 µN/um.

The fiber radius for 15% w/v PCL, PCL/PLGA blends of 75/25 and 50/50, were 1.029 µm, 0.788 µm and 0.510 µm, respectively. Using equations (A.2) and (A.3), the average dF/dz for each blend obtained from Figure A-4, and assuming that the value for L is constant for the fibers, we calculate the relative Young's Modulus for the fibers.

The results in Table A-1 indicate that PCL has the lowest bending modulus. When PLGA is added, the bending modulus increases, that is to say fiber stiffness increases. These results concur with literature (Baker et al., 2009; Shim et al., 2015; Bosworth, 2011; Chen et al, 2013).

Table A-1: Values of the relative bending modulus (E) calculated for each of the electrospun fibers of PCL and PCL/PLGA (75/25 and 50/50).

	PCL	PCL/PLGA 75/25	PCL/PLGA 50/50
r (μm)	1.029	0.788	0.510
dF/dz (μN/μm)	24.09	17.28	18.91
$E_{relative}$	0.569	1.187	7.414

References

Baker, B., Nerurkar, N., Burdick, J., Elliot, D., Mauck, R. (2009). Fabrication and modeling of dynamic multi-polymer nanofibrous scaffolds. *Journal of Biomechanical Engineering*, 131(10), 1-22.

Bosworth, L., Downes, S. (2011). Electrospinning for Tissue Regeneration. Elservier.

Cappella, B., & Dietler, G. (1999). Force-distance curves by atomic force microscopy. *Surface Science Reports*, *34*(1-3), 1–104.

Chen, L., Bai, Y., Liao, G., Peng, E., Wu, B.,Wang, Y., Zeng, X., Xie, X. (2013). Electrospun Poly(L-lactide)/Poly(ε-caprolactone) Blend Nanofibrous Scaffold: Characterization and Biocompatibility with Human Adipose-Derived Stem Cells. *PloS ONE* 8(8), 1-9.

Croisier, F., Duwez, a. S., Jérôme, C., Léonard, a. F., Van Der Werf, K. O., Dijkstra, P. J., & Bennink, M. L. (2012). Mechanical testing of electrospun PCL fibers. *Acta Biomaterialia*, *8*(1), 218–224.

Safanama, D., Marashi, P., Hesari, A., Firoozi, S., Aboutalebi, S., Jalilzadeh, S. (2012). Elastic modulus measurement on nanocomposite materials by atomic force microscopy. Int. J, Mod, Phys. Conf. Ser, 5, 502-509.

Shim, J., Won, J., Sung, S., Lim, D., Yun, W., Jeon, Y., Huh, J. (2015). Comparative Efficacies of a 3D printed PCL/PLGA/β-TCP Membrane and a titanium membrane for guided bone regeneration in beagle dogs, *Polymers*, 7(10), 2061-2077.